

See discussions, stats, and author profiles for this publication at: <https://www.researchgate.net/publication/223576466>

On the nature of lead–lag relationships during glacial–interglacial climate transitions

ARTICLE *in* QUATERNARY SCIENCE REVIEWS · DECEMBER 2009

Impact Factor: 4.57 · DOI: 10.1016/j.quascirev.2009.09.019

CITATIONS

43

READS

261

2 AUTHORS:



[Andrey Ganopolski](#)

Potsdam Institute for Climate Impact Rese...

149 PUBLICATIONS **7,938** CITATIONS

[SEE PROFILE](#)



[Didier M. Roche](#)

VU University Amsterdam

118 PUBLICATIONS **1,486** CITATIONS

[SEE PROFILE](#)



On the nature of lead–lag relationships during glacial–interglacial climate transitions

Andrey Ganopolski^{a,*}, Didier M. Roche^{b,c,1}

^a Potsdam Institute for Climate Impact Research, P.O. Box 601203, D-14412 Potsdam, Germany

^b Laboratoire des Sciences du Climat et de l'Environnement, LSCE/IPSL, Laboratoire CEA/CNRS/UVSQ, CE Saclay, l'Orme des Merisiers, F-91191 Gif-sur-Yvette Cedex, France

^c Section Climate Change and Landscape Dynamics, Department of Earth Sciences, Vrije Universiteit Amsterdam, De Boelelaan 1085, 1081 HV Amsterdam, The Netherlands

ARTICLE INFO

Article history:

Received 18 August 2008

Received in revised form

10 September 2009

Accepted 17 September 2009

ABSTRACT

Analysis of leads and lags between different paleoclimate records remains an important method in paleoclimatology, used to propose and test hypotheses about causal relationships between different processes in the climate system. The robust lead of Antarctic temperature over CO₂ concentration during several recent glacial–interglacial transitions inferred from the Antarctic ice cores apparently contradicts the concept of CO₂-driven climate change and still remains unexplained. Here, using an Earth system model of intermediate complexity and generic scenarios for the principal climatic forcings during glacial–interglacial transitions we performed a suite of experiments that shed some light on the complexity of phase relationships between climate forcing and climate system response. In particular, our results provide an explanation for the observed Antarctic temperature lead over CO₂ concentration. It is shown that the interhemispheric oceanic heat transport provides a crucial link between the two hemispheres. We demonstrate that temporal variations of the oceanic heat transport strongly contribute to the observed phase relationship between polar temperature records in both hemispheres. It is shown that the direct effect of orbital variations on the Antarctic temperature is also significant and explains the observed cooling trend during interglacials. In addition, an imbedded $\delta^{18}\text{O}$ model is used to demonstrate that during glacial–interglacial transitions, the temporal evolution of deep calcite marine $\delta^{18}\text{O}$ in different locations and at different depths can considerably deviate from that implied by the global ice volume change. This finding indicates that the synchronization of different marine records by means of foraminiferal calcite $\delta^{18}\text{O}$ yield large additional uncertainties. Based on our results, we argue that the analysis of leads and lags alone, without a comprehensive understanding and an adequate model of all relevant climate processes, cannot provide direct information about causal relationships in the climate system.

© 2009 Elsevier Ltd. All rights reserved.

1. Introduction

Analysis of the lead–lag (phase) relationships between different paleoclimate records remains one of the principal tools used in paleoclimatology to propose and to test hypotheses about the mechanisms of past climate change (e.g., Alley et al., 2002; Broecker, 2003). The method is directly based on the fundamental physical principle of causality, which in short can be formulated as follows: each effect has its cause and the cause precedes the effect. Strictly speaking, the physical principle of

causality can only be applied when presumable cause and its effect are clearly separated in time and then, only to falsify the hypothesis about the causal relationship. Namely, that if event B occurs later than event A, then the effect B cannot be the cause of event A (Fig. 1a). The lead of event A, of course, cannot alone prove that this is the cause for the event B. A good example for using the causality principle to falsify hypotheses about causal links between two paleoclimate events is the relative timing of meltwater pulse 1A (MWP-1A) and the onset of a warm Bølling event. If these two events occurred approximately simultaneously (within the dating errors) it is possible that MWP-1A was the cause of Bølling, as suggested by Weaver et al. (2003). However, if the recent dating of MWP-1A by Stanford et al. (2006) is correct, which implies that MWP-1A occurred ca 500 years after the onset of Bølling, then MWP-1A cannot be considered as a potential cause of Bølling.

* Corresponding author.

E-mail address: andrey@pik-potsdam.de (A. Ganopolski).

¹ Also at the Department of Paleoclimatology and Geomorphology, Vrije Universiteit Amsterdam, De Boelelaan 1085, NL-1081 HV Amsterdam, The Netherlands.

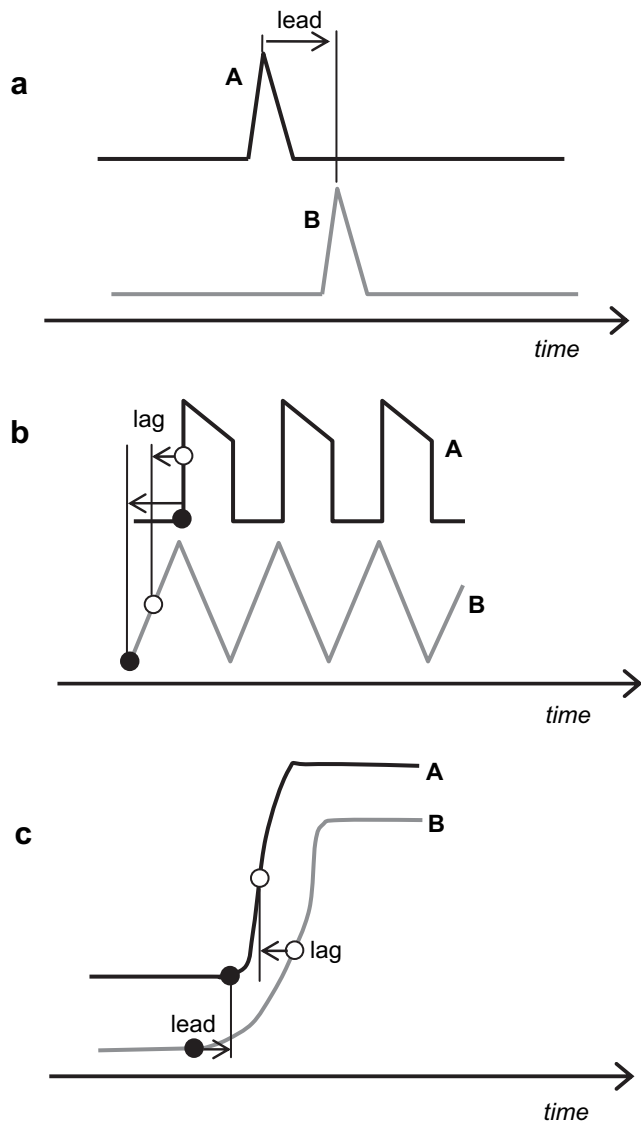


Fig. 1. Different types of paleoclimate “events” and associated leads and lags discussed in the text. Open circles correspond to midpoint of transition and filled circles – to the “onset” of transition. Lags and leads are defined for the record “A” compared to the record “B”.

In the (usual) case, when paleoclimatological events are not well separated in time or when there is a sequence of events, not only the interpretation but even the definition of leads and lags becomes ambiguous (Fig. 1b). For example, a direct correlation between Dansgaard–Oeschger (D–O) events recorded in Greenland and Antarctic warm events implies Antarctic temperature leads by ca 1000 years (Blunier et al., 1998), which apparently rules out a possibility that Antarctic warm events are caused by D–O events. However, if one performs the analysis based on the mechanisms of Atlantic seesaw (Crowley, 1992), then the temporal dynamics of Antarctic temperature and one-to-one correspondence between warmings in both hemispheres (EPICA Community Members, 2006) is readily explained by changes in the interhemispheric ocean transport forced from the north and a large thermal inertia of the Southern Ocean (Ganopolski and Rahmstorf, 2001; Stocker and Johnsen, 2003).

When climate change on orbital time scales is concerned, the use of the lead–lag relationship to detect the cause and effect becomes even more complicated. Indeed, climate changes on

orbital time scales cannot be considered as “events”, but rather as continuous variations which occur more or less synchronously at different locations and in different proxies. As was discussed by Alley et al. (2002), even the sign of the phase between different paleoclimate record depends on whether the beginning or midpoint of the transition is chosen to determine leads and lags (Fig. 1c). Alley et al. (2002) argued that the beginning of the transition is more important for the casual relationship. However, it is usually very hard to identify the beginning of the transition within the noisy paleoclimate records. In practice, either midpoints of transition or maximum correlations are used to determine lead–lag relationships between paleoclimate records.

An additional complication for using lead–lag analysis of the paleoclimate records to deduce causal relationship stems from the fact that past climate changes were caused by several climate forcings of comparable importance. For example, for the Last Glacial Maximum (ca 21,000 years BP) it has been shown (Hewitt and Mitchell, 1997; Ganopolski, 2003; Schneider von Deimling et al., 2006) that radiative forcing caused by changes in the ice sheets, atmospheric concentration of greenhouse gases, vegetation cover and atmospheric dust are globally of comparable magnitude ($1\text{--}3\text{ W/m}^2$) but the spatial patterns of temperature responses to these factors are very different. Moreover, the temporal dynamics of these forcings during the glacial–interglacial transition were rather different as well. Therefore, the phase relationship between paleoclimate records from different regions may simply reflect the differences in temporal dynamics of dominant regional forcings, rather than provide any sensible information about causal relationships.

The phase relationship between temperature and CO_2 concentration, inferred from the Antarctic ice cores, represents an example of a potential problem associated with the interpretation of leads and lags. Analysis of the Antarctic ice cores produced robust and rather unexpected result that the Antarctic temperature led CO_2 concentration by ca 1000 years during previous glacial–interglacial transitions. In particular, Fischer et al. (1999) found 600 ± 400 years temperature lead over CO_2 concentration during the past three glacial terminations. Similarly, 800 ± 600 years temperature lead was reported for Termination I by Monnin et al. (2001), 800 ± 200 years for Termination III by Caillon et al. (2003), and Siegenthaler et al. (2005) found temperature leads of 800, 1600, and 2800 years during Terminations V, VI, VII, respectively. These results caused some confusion because when taking into account the large thermal inertia of the Southern Hemisphere, one would rather expect a detectable temperature lag behind CO_2 concentration if the latter is the principal cause of temperature changes in the Southern Hemisphere. Unsurprisingly, this fact was used by climate skeptics to challenge the role of CO_2 in climate change.

Here, using an Earth system model of intermediate complexity forced by a generic (i.e., a rather simplified and schematic) scenario for a glacial–interglacial–glacial transition, we argue that the Antarctic temperature lead over the CO_2 concentration can be readily explained as a transient response to a combination of several climatic forcings and hence does not impose any problem for the concept of the leading role of CO_2 in past and future climate changes. It is also shown that the “southern lead” does not imply the leading role of the Southern Hemisphere in driving the glacial cycles. Rather, it can be explained as a direct response to the “northern” and global forcings. Results of the analysis of the temporal dynamics of the relative ^{18}O isotope concentration in sea water during the glacial–interglacial transitions reveal another potential problem in the interpretation of paleoclimate proxies. Namely, it is shown that $\delta^{18}\text{O}$, which is often interpreted as the proxy for global ice volume and is widely used for synchronization

of different paleoclimate records, could lead or lag the global ice volume considerably, depending on the location.

2. Method

For this study the Earth system model of intermediate complexity CLIMBER-2 (Petoukhov et al., 2000) was used. The model consists of a 2.5-dimensional statistical-dynamical atmosphere model, a land surface module, a dynamical vegetation model and a zonally-averaged, three-basin ocean model, which also includes a sea ice component. Atmospheric, land surface and vegetation components have spatial resolutions of $51^\circ \times 10^\circ$, and the ocean component has a meridional resolution of 2.5° and 21 unevenly distributed layers. The model explicitly accounts for all major climate feedbacks (water vapor, lapse rate, cloud, albedo) and does not employ any type of flux correction. The CLIMBER-2 dynamical ice sheet component was not used in the present study. Instead, the temporal evolution of the ice sheet distribution was prescribed, and expressed in terms of the fraction of each model grid cell covered by ice and its elevation. The dynamical vegetation model (Brovkin et al., 2002) was active and hence the climate-vegetation feedback was explicitly accounted for in all experiments.

In this study we make use of the CLIMBER-2 oxygen-18 module as an additional step towards a tighter data-model comparison. The module used here is identical to that developed by Roche et al. (2004a). It includes the effect of large-scale transport and fractionation of ^{18}O in the atmosphere from evaporation at the atmosphere–ocean boundary to precipitation as rain or snow. Accounting for ^{18}O in the river runoff enables us to close the atmospheric–isotopic water budget. Additionally, ^{18}O is transported in the ocean, following advection and mixing of the water masses. It is assumed that there is no large-scale storage of ^{18}O in sea ice. The oxygen-18 module has already been validated under present-day boundary conditions (Roche et al., 2004a) and used in several palaeoclimate studies (e.g., Roche et al., 2004b). As we compute both the oceanic temperature and $\delta^{18}\text{O}$ evolutions, we are able to simulate $\delta^{18}\text{O}$ of the calcite from standard linear relationships (Shackleton, 1974).

The CLIMBER-2 model has been used in different configurations for a variety of studies of past and future climate changes. Comparison of model simulations with observational and paleoclimate data, and the results of state-of-the-art coupled GCMs, shows that in spite of a coarse spatial resolution and considerable simplifications in treatment of many processes in the climate system, the CLIMBER-2 model has reasonable skill in simulating the climate system response to different forcings on global and continental scales (Ganopolski et al., 2001; Petoukhov et al., 2005). CLIMBER-2 has a climate sensitivity of 2.7°C to a doubling of CO_2 concentration, which is close to the middle of the IPCC range and its sensitivity to anomalous freshwater forcing is within the range of coupled GCMs and models of intermediate complexity employing 3-D ocean components (Rahmstorf et al., 2005; Stouffer et al., 2006).

Since the aim of this work is to study the nature of lead–lag relationships between climate forcings and climate responses during the glacial–interglacial transitions, we are only concerned here with the part of the glacial cycle which encompasses the glacial termination, the interglacial and the glacial inception. For the sake of simplicity in the interpretation of modeling results, we intentionally employed a rather schematic (generic) scenario for the temporal evolution of the principal climate forcings during the glacial–interglacial transitions instead of using real paleoclimatological data for any specific glacial cycle. Moreover, the latter would only be possible with sufficient accuracy for the last glacial termination. At the same time, as is shown below, the

simulations performed with these rather schematic scenarios capture a number of important features seen in the paleoclimate records.

We consider three major forcings relevant to the glacial–interglacial transitions: greenhouse gases concentration, ice sheets and orbital forcing. Since CO_2 is by far the most important greenhouse gas during glacial–interglacial changes, we consider changes in CO_2 concentration only. We applied a very simple scenario for the atmospheric CO_2 concentration: a linear growth during the glacial termination, a constant value during the interglacial state and a linear decrease during the glacial inception (Fig. 2).

The second set of forcings is related to the waning and waxing of the Northern Hemisphere ice sheets. For simplicity, changes in the area and elevation of the Antarctic Ice Sheet were ignored in our study except for the changes in elevation associated with the global sea level variations. We prescribed temporal evolution of the Northern Hemisphere ice volume to be identical in shape to that of CO_2 concentration, i.e., when appropriately scaled, the CO_2 concentration and the ice volume graphs are identical (Fig. 2). Hereafter, we will refer to both of these forcings as the “generic

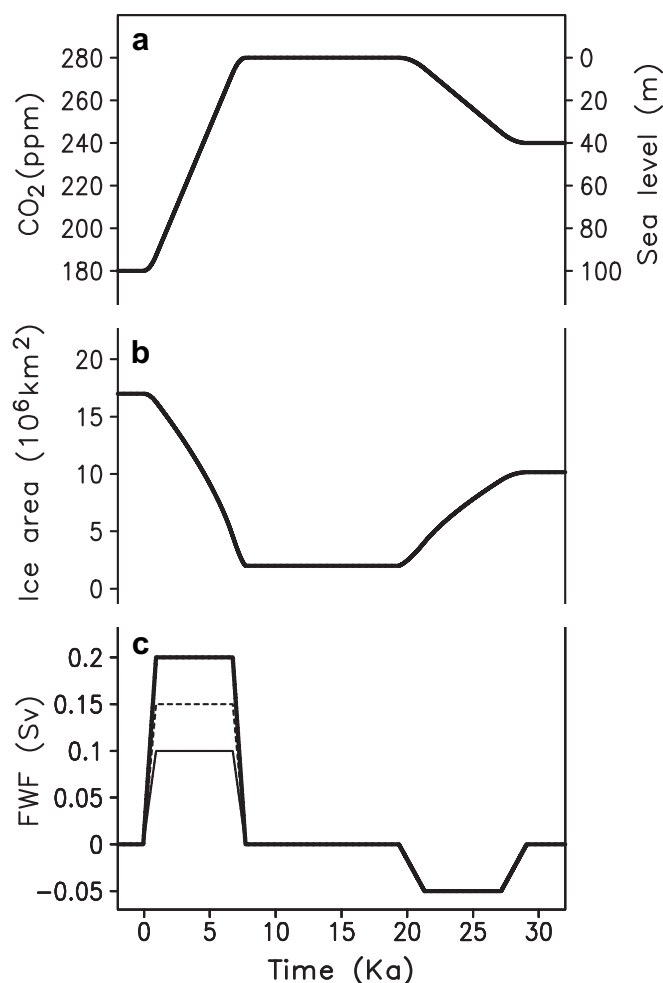


Fig. 2. “Generic” forcing scenarios used in different experiments. (a) CO_2 concentration and the global ice volume expressed in terms of sea level. (b) Area of the ice sheet in the Northern Hemisphere. (c) Anomalous freshwater flux applied in the Northern Hemisphere. Solid line corresponds to the temporal derivative of the global ice volume and used in experiment labelled by “0.20”, dashed line corresponds to the freshwater forcing used in experiments labelled by “0.15” and thin line corresponds to the experiments labelled by “0.10”.

forcing” (GF). The direct implication of this setup is that there is no prescribed lead or lag between CO₂ and ice volume variations.

Changes in the ice volume directly affect climate via changes in sea level, ocean area, surface albedo, elevation, and freshwater flux into the ocean associated with melting of the ice sheets and iceberg calving. The effect of sea level change on land surface temperature is explicitly accounted for in the CLIMBER-2 model. The effect related to the reduction of ocean area during glacial time was neglected in our simulations, i.e., land/ocean distribution was held constant in all experiments. The other three effects of the ice sheets on climate, namely, via changes of the surface albedo, ice sheet elevation and anomalous freshwater flux into the ocean, are also related to the total ice volume but in a more complex manner. Since CLIMBER-2 is a geographically explicit model, the total ice volume should be distributed over a number of grid cells. Spatial distribution and elevation of the ice sheets at the glacial maximum (i.e., before the termination) was taken to be the same as in our previous simulations of the Last Glacial Maximum (e.g., Ganopolski et al., 1998). We also assumed that the area of the Northern Hemisphere ice sheets is proportional to the power 2/3 of the ice volume. Assuming in addition that bedrock depression under the ice sheet is equal to 1/3 of the ice sheet thickness, a rather simplistic scenario for the retreat of the ice sheets during the termination and the ice sheets advance during the glacial inception was constructed.

The global anomalous freshwater flux into the ocean due to growth or decay of the ice sheets is equal to the temporal derivative of the global ice volume. This flux, however, must be distributed regionally. Here we assume that the whole freshwater flux associated with melting of the ice sheets during the glacial termination is uniformly distributed in the North Atlantic between 50 and 70°N, whilst during the ice sheets’ growth, 2/3 of the anomalous (negative) flux was extracted from the same area of the Northern Atlantic and the rest from the Northern Pacific. This anomalous freshwater flux was added to that simulated by the climate model as a sum of precipitation, evaporation and runoff. Note that the freshwater flux in the climate model is computed on the assumption that the ice sheets are in equilibrium, i.e., the total freshwater flux into the ocean equals zero.

The so-called “orbital forcing” determined by the Earth’s orbital parameters was held constant in all but two experiments. In these two experiments (CIO.20 and CIO.10, see Table 1) the orbital parameters (eccentricity, precession and obliquity) varied in time the same way as during penultimate glacial–interglacial–glacial transition MIS6–5 (exp. CIO.20) or during the last termination and Holocene (exp. CIO.1). The last experiment also differs from others by its shorter duration.

For the interpretation of modeling results, it is important to note that all forcings in our experiments were either applied solely in the Northern Hemisphere (ice sheets, freshwater flux) or were

approximately hemispherically symmetric, such as radiative forcing of CO₂, sea level and obliquity induced changes in annual insolation. The only hemispherically asymmetric forcing is the precessional component of the orbital forcing. Since precessional variations do not affect annual insolation, this component of the orbital forcing has little effect on annual temperature in the Southern Hemisphere. It produces a stronger effect on the annual temperature in the Northern Hemisphere via the vegetation feedback (e.g., Claussen et al., 2006), but it is still rather small compared to other climate forcings. Thereby, the Southern Hemisphere temperature lead over the Northern Hemisphere is not included into prescribed forcings. As will be shown below, the “southern lead” results from the complex response of the Southern Hemisphere to the Northern Hemisphere and hemispherically symmetric forcings.

All experiments were performed using as initial climate conditions the equilibrium climate state corresponding to the fixed boundary conditions prior to the glacial–interglacial transition. Note that these boundary conditions were different in different experiments. To obtain an equilibrium state, the model was run for 5000 years with a constant CO₂ concentration, ice sheets, zero anomalous freshwater flux and constant orbital configuration (see Table 1). The model was then run for 35,000 years using different sets of climate forcings. The onset of the G–I transition corresponds to the model year 3000, but for convenience in all figures, 3000 years offset is introduced on time axes such that the timing of the beginning of glacial–interglacial transition corresponds to “0” and the end of the interglacial–glacial transition corresponds to the year 25,000.

Below we will primarily analyze annual mean temperature change in the Eastern Antarctic sector (hereafter called “Antarctic temperature”) and in the grid cell covering the North Atlantic sector between 60 and 70°N (hereafter called the “Greenland temperature”). The leads and lags between these two temperatures and GF were determined by two different methods, which are widely used in paleoclimatology. In the first one, the leads (lags) were determined as the difference between the timing of midpoint of deglacial climate change and the timing of midpoint of GF change during glacial termination which corresponds to the year 4000 (Fig. 2). The midpoint for temperature was determined as the timing of warming by one half of the difference between the temperature prior to the termination and the maximum temperature reached after the termination. In the second method the leads (lags) were determined as the time offset between GF and temperature which gives the maximum correlation between GF and temperature during the whole glacial–interglacial–glacial transitions, i.e., during the time interval from 0 to 25,000 years.

3. Equilibrium climate response to climate forcings associated with glacial–interglacial transitions

In this work we consider four principal forcings which determine climate change during glacial–interglacial transitions: the waning and waxing of the Northern Hemisphere ice sheets, anomalous freshwater flux associated with changes in the ice sheet volume, changes in the atmospheric CO₂ concentration and orbital forcing. In this section, we analyze the role of individual forcings by studying equilibrium response of the climate system to individual forcing. This analysis is similar to the factor analysis performed in Ganopolski (2003) except that here, we consider vegetation changes as a feedback rather than individual forcing.

Fig. 3a shows the equilibrium response of annual mean surface air temperatures to the lowering of CO₂ from 280 to 180 ppm for the interglacial boundary conditions, i.e., without Northern Hemisphere continental ice sheets. Similar to numerous previous

Table 1
Experimental setup.

Experiment	Ice sheets and sea level	Maximum freshwater flux during glacial termination	Orbital forcing
C	Constant PD	0	Constant PD
O	Constant PD	0	146–111 ka BP
CI.10	Time-dependent	0.1 Sv	Constant PD
CI.15	Time-dependent	0.15 Sv	Constant PD
CI.20	Time-dependent	0.2 Sv	Constant PD
CI.20D	Time-dependent (ice volume lags CO ₂ by 2000 years)	0.2 Sv	Constant PD
CIO.10	Time-dependent	0.1 Sv	22–0 ka BP
CIO.20	Time-dependent	0.2 Sv	146–111 ka BP

studies, it shows a relatively zonal and hemispherically symmetric cooling with pronounced polar amplification of the response. The response to CO₂ changes for glacial conditions, i.e., for the maximum ice sheet extent, is rather similar (not shown). In both cases, globally averaged temperature is lowered by about 2 °C, and in the high latitudes of both hemispheres by about 3–4 °C.

Fig. 3b shows the equilibrium response of annual mean surface air temperatures to imposed changes in the ice sheet extent in the Northern Hemisphere and global change in land elevation due to sea level drop. The prescribed Northern Hemisphere ice sheets correspond to the global sea level drop by 100 m, which is equivalent to the rise of land above sea level by the same 100 m. The latter results in the temperature drop over land even without any additional forcings. In a separate experiment (not shown), we found that a uniform increase of land elevation by 100 m results in temperature drop over Antarctica by ca 0.5 °C which is close to what one can expect from the lapse rate effect, although, in general,

the magnitude of temperature response over the continents can deviate considerably from this figure. As is seen in Fig. 3b, the largest cooling due to imposed ice sheets occurs over the ice sheets, where a strong elevation effect (due to elevation rise by several kilometers), combined with changes in surface albedo, cause cooling by up to 20 °C. The strong cooling extends well beyond the area of imposed ice sheets, but rapidly diminished towards equator. However, in the high latitudes of the Southern Hemisphere, the cooling increases considerably and exceeds 2 °C over Antarctica. Since no change in surface albedo is directly prescribed in the Southern Hemisphere and, as was discussed above, changes in surface elevation due to sea level drop can explain only 0.5 °C, this strong cooling can only be attributed to the interhemispheric teleconnections. Analysis of the climate system energetics show that changes in atmospheric transport contribute a small amount to the cooling of the Southern Hemisphere, while an increase of the Atlantic meridional heat transport (by about 0.2 PW at the Equator)

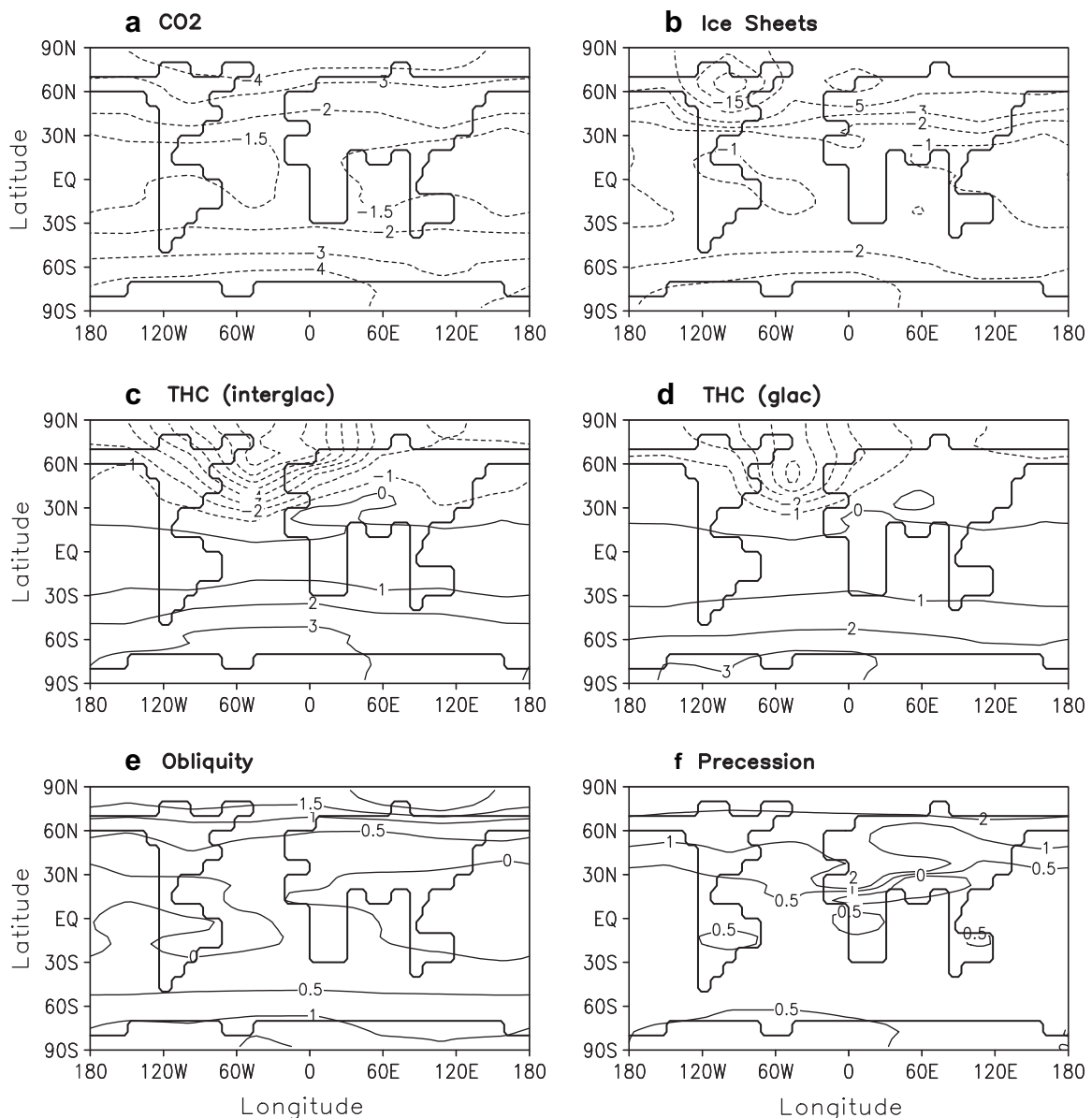


Fig. 3. Mean annual equilibrium surface air temperature response to: (a) lowering of CO₂ concentration from 280 to 180 ppm; (b) imposing of the glacial ice sheets and orography change; (c) shutdown of the AMOC under present-day climate conditions; (d) shutdown of AMOC under glacial climate conditions; (e) maximum obliquity changes (i.e., the difference between obliquity angles $\epsilon = 24^\circ$ and $\epsilon = 22.5^\circ$); and (f) maximum precessional change (i.e., “warm” minus “cold” orbit).

plays the major role. Since the rate of overturning circulation increases insignificantly with the imposed ice sheets, in comparison with interglacial state, the intensification of northward heat transport must be attributed to changes in the vertical temperature structure. Indeed, the meridional oceanic heat transport due to the overturning circulation is proportional to the strength of the overturning and the temperature difference between the upper and the lower branches of the overturning circulation. Imposed ice sheets cause a pronounced cooling of the lower branch of the circulation (NADW), whilst the temperature of the upper branch outside of the high latitudes of the Northern Hemisphere is much less affected. As a result, the temperature difference between the upper and the lower branches increases by ca 20% which causes a similar increase in the interhemispheric heat transport. Therefore, the Northern Hemisphere cooling, directly imposed via changes in surface albedo, causes a symmetric response (i.e., cooling) in the Southern Hemisphere via changes in the oceanic heat transport. Note that this effect is opposite to the well-known interhemispheric seesaw mechanism when the Northern Hemisphere cooling, resulting from the weakening of the meridional overturning circulation, is accompanied by a Southern Hemisphere warming. It will be argued below that the first mechanism contributes to the bipolar response during the onset of the glacial state, while the latter plays an important role during the glacial termination.

Imposing a constant freshwater flux into the Northern Atlantic with a magnitude corresponding to the melting rate of the Northern Hemisphere ice sheets during deglaciation, i.e., 0.2 Sv, leads to an almost complete shutdown of the AMOC both under present-day and glacial conditions. However, the temperature response in the Northern Hemisphere differs considerably between these two experiments (Figs. 3c,d), which is in-line with our previous findings (Ganopolski et al., 2001; Ganopolski and Rahmstorf, 2001). The main difference is that in the glacial climate state, the Northern Hemisphere cooling in response to shutdown of the AMOC is weaker and the maximum cooling is located considerably more southward compared to the interglacial state. This is explained by a smaller Atlantic northward transport from middle to high latitudes under the glacial climate state. The pronounced warming over the South Atlantic and Southern Ocean is explained by the interhemispheric seesaw mechanism (Crowley, 1992). It is important to note that Figs. 3c,d represent equilibrium temperature response to the complete shutdown of AMOC. The transient response differs considerably between the two hemispheres – the cooling of the Northern Atlantic in response to the shutdown of the AMOC occurs on decadal time scale while warming over the Southern Ocean and Antarctica develops much slower and reaches an equilibrium only after several thousand years.

To clarify the role of orbital forcing in the bipolar temperature variations during glacial–interglacial transitions, we performed two pairs of equilibrium sensitivity experiments in which we change only one of two major components of the orbital forcing – climatic precession and obliquity. The Earth's eccentricity in all these experiments was kept constant at the value of 0.05 corresponding to its value during MIS5e and which is close to the maximum value of eccentricity. In the first pair of experiments we prescribed two different obliquity values of 22.5° and 24°, which are close to the minimum and the maximum values of obliquity, respectively. Due to the fact that variations in obliquity have a relatively constant amplitude, simulated changes are representative for any obliquity cycle during Quaternary. As shown in Fig. 3e, an increase of obliquity leads to widespread annual warming, with the strongest warming in high latitudes of both hemispheres. This is explained by the fact that under the high obliquity, annual mean insolation at the poles is up to 20 W/m² higher than for the low obliquity. This increase in insolation in high latitudes is compensated by the lowering of insolation in

low latitudes and globally averaged insolation remains unaffected by obliquity changes. However, due to stronger climate feedbacks operating in the high latitudes, the effect of obliquity on the global mean temperature is not cancelled and the globally averaged SAT is higher by 0.5 °C for the high obliquity. Still, changes at the higher latitudes are much larger, the annual temperature over Antarctica being about 1.5 °C higher in the experiment with high obliquity. Interestingly enough, this figure is consistent with the results of early work by Harvey (1989).

Since obliquity directly affects annual mean insolation, annual SAT response to obliquity change can be explained in the first approximation as a linear climate response. To the contrary, while changes in precessional angle strongly affect insolation in different seasons, they do not affect the annual mean insolation. Therefore, change in annual SAT resulting from variations of precession can only be explained by a non-linear response in the Earth system. To better comprehend the climate response to a change in precession, we performed two experiments with the same value of obliquity (held at 23°) and precessional angles set at –90° and 90°. The former corresponds to the orbital configuration where the summer equinox coincides with perihelion and, hence, to the maximum summer insolation in the Northern Hemisphere, commonly referred to as “warm orbit”. The latter corresponds to the orbital configuration when summer equinox coincides with aphelion and, hence, minimum summer insolation in the Northern Hemisphere (“cold orbit”). As shown in Fig. 3f, this non-linear response is of comparable magnitude with that obtained for obliquity variations. Part of this response is attributed to the vegetation feedback, as discussed in Claussen et al. (2006). However, this mechanism can not explain why the Antarctic temperature is higher (by about 0.5 °C) for the “warm orbit” since summer insolation is at minimum in the Southern Hemisphere for this orbital configuration. A set of additional experiments (not shown here) reveals that approximately half of this warming results from a non-linear local temperature response to the insolation changes whilst another half is due to change in the interhemispheric oceanic heat transport. Therefore, our results agree qualitatively with the recent work by Huybers and Denton (2008), who argued that the synchronous bipolar response to precessional variations results from local Antarctic temperature response to seasonal insolation changes.

4. Transient simulations of glacial–interglacial–glacial transitions

4.1. GHGs only experiment

To better understand the role of the different climate forcings during glacial–interglacial transition we performed a set of experiments adding one forcing after another. We start our analysis from an experiment where only the atmospheric CO₂ concentration varies while the interglacial distribution of the ice sheets and orbital parameters are kept constant (experiment C). Results of this experiment are shown in Fig. 4. The magnitude of glacial–interglacial temperature changes in Antarctica is about 4.5 °C, i.e., half of the range of observed glacial–interglacial Antarctic temperature variations (Jouzel et al., 2003). When applying midpoint criteria, a time lead of Antarctic temperature over GF of about 200 years is found (Table 2). This fact is surprising at first glance, as one would expect a lag of the Antarctic temperature because of a long response time of the Southern Hemisphere temperature. The explanation of this fact is, however, rather straightforward: the radiative forcing of CO₂ is proportional not to the concentration but to the logarithm of CO₂ concentration (dashed line in Fig. 4b). Thereby during the CO₂ rise, its radiative forcing leads the concentration and lags it during the CO₂ decrease. Hence, as one should expect, Antarctic

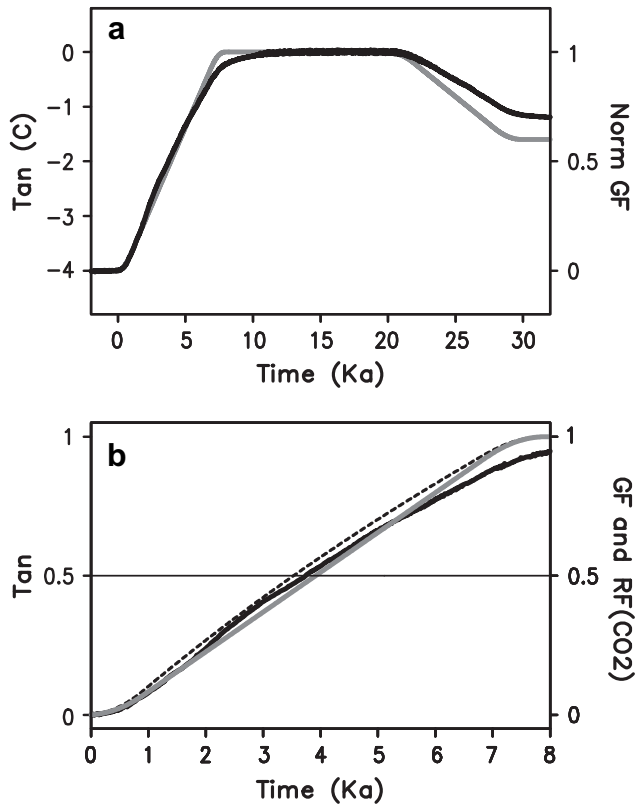


Fig. 4. Temporal evolution of the annual mean Antarctic temperature anomalies (black line) compared to arbitrarily scaled GF (grey line) in the experiment C during the whole experiment (a) and during the glacial termination (b). In panel (b), the Antarctic temperature is normalized the same way as GF and the dashed line shows normalized radiative forcing of CO₂.

temperature lags behind radiative forcing but leads GF during the glacial–interglacial transitions. If, however, the phase relationship is determined for the whole glacial–interglacial–glacial transition using the maximum correlation method, then GF leads temperature by about 800 years which is explained by a considerable lag of temperature during the glacial inception and a difference in the shape of the Antarctic temperature and GF.

4.2. Effect of the ice sheets and freshwater forcing

Changes in the ice sheet distribution, global sea level and associated freshwater flux are added to the CO₂ variations in Exp. CI.20. The last number in the experiment acronym refers to the maximum anomalous freshwater flux during the glacial

Table 2

Leads/lags between Antarctic and Greenland temperatures and the generic forcing during glacial termination and complete glacial–interglacial transitions computed using the “midpoint” and the maximum correlation methods.

Experiment	Antarctic temperature lead (lag) in years		Greenland temperature lead (lag) in years	
	Termination midpoint	Max correlation	Termination midpoint	Max correlation
C	200	–800	350	–510
CI.20	1340	1650	–3120	–1810
CI0.20	940	2330	–2930	–1140
CI.20D	230	820	–2950	–3030
CI.15	1410	1230	–1350	–1430
CI.10	300	1550	460	–10
CI0.10	280	–	450	–

termination, which is equal to 0.2 Sv (1 Sv = 10⁶ m³/s) in this experiment (Fig. 2). Orbital forcing was again kept constant. Introducing an additional 0.2 Sv of freshwater flux into the northern North Atlantic during glacial termination leads to a nearly complete shutdown of the AMOC during the whole glacial termination (Fig. 5c). Only after a decrease of anomalous freshwater flux does the AMOC abruptly recover. The weakening of the AMOC leads to a reduction in the cross-equatorial northward oceanic heat transport by about 0.5 PW (1 PW = 10¹⁵ W) that implies an equal energy gain for the Southern Hemisphere, causing an additional warming there due to the “interhemispheric seesaw” mechanism. Changes in the interhemispheric ocean heat transport closely followed the strength of the AMOC except for the period of the AMOC overshoot at the end of the glacial termination. This additional Southern Hemispheric warming due to the reduction of the interhemispheric energy transport, added on top of an almost linear warming trend caused by CO₂ and sea level rise, explains a considerable Antarctic temperature lead over GF. Indeed, both methods for lead/lag determination give more than 1000 years Antarctic temperature lead over GF in experiment CI.20 (Table 2). Apart from a more abrupt warming, Antarctic temperature response is also characterized by a considerable overshoot above its

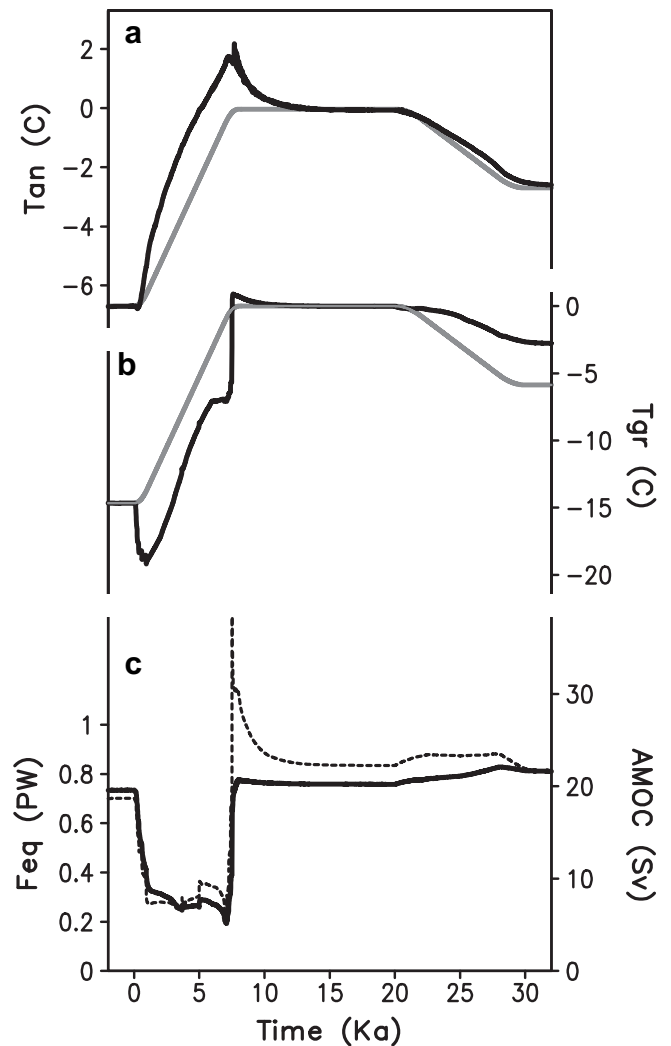


Fig. 5. Temporal evolution of annual mean climate characteristics in the experiment CI.2. (a) Antarctic temperature anomalies and (b) Greenland temperature anomalies (black lines) compared to arbitrarily scaled GF (grey line). (c) Maximum of the AMOC (dashed line) and cross-equatorial northward oceanic heat transport (solid line).

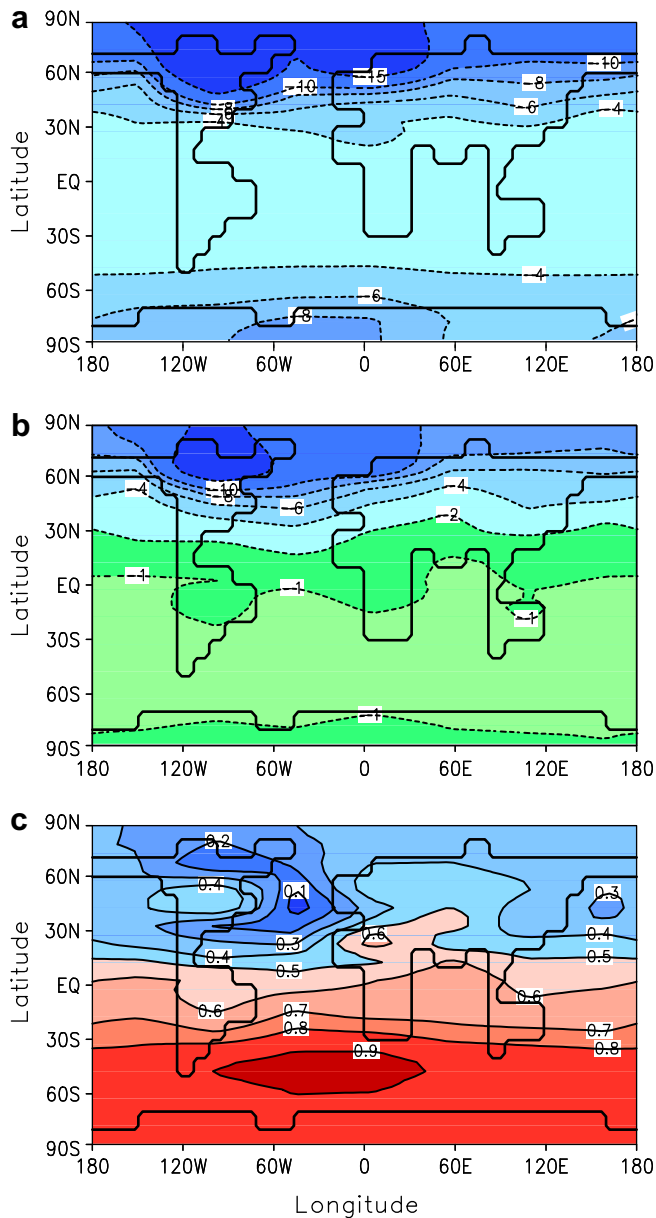


Fig. 6. Annual mean surface air temperature differences in °C in the experiment CI.2 between (a) equilibrium glacial and interglacial states; (b) between midpoint of the glacial termination and the interglacial state; and (c) the ratio between the temperature rise at the midpoint of termination and interglacial to glacial temperature difference.

equilibrium interglacial value by nearly 2 °C (Fig. 5a). The magnitude of the overshoot is similar to the equilibrium Antarctic temperature response to a complete shutdown of the AMOC in the CLIMBER-2 model water hosing experiment described in previous section. As soon as the AMOC resumes, the Antarctic temperature drops to its equilibrium interglacial value with a typical time scale of about 1000 years.

During the glacial inception in experiment CI.20, the normalized Antarctic temperature follows GF more closely than in experiment C and Antarctic cooling in CI.20 exceeds the cooling in experiment C by more than 1 °C during the glacial inception. Since only 0.3 °C of this additional cooling can be directly attributed to the effect of sea level drop and since no additional forcings have been applied to the Southern Hemisphere in this experiment compared to experiment C, the origin of this additional cooling must be related to changes in

the Northern Hemisphere. As was discussed in the previous section, most of this additional cooling in the Southern Hemisphere is explained by an increase of the ocean heat transport, caused by a cooling produced by the Northern Hemisphere ice sheets. As is shown in Fig. 5c, during glacial inception, the interhemispheric Atlantic heat transport increased by 0.1 PW causing additional cooling in the Southern Hemisphere. Two factors contribute to this increase in interhemispheric ocean heat transport. The first is related to a modest intensification of the AMOC, attributed to the cooling and increased salinity of the North Atlantic deep water (NADW) during glacial inception, which enhances the meridional density gradient across the Atlantic Ocean. Another factor, as was discussed in the previous section, is related to the increased temperature difference between the upper and the lower branches of AMOC.

As seen in Fig. 5b, the temporal dynamics of the Greenland temperature in experiment CI.20 differ considerably from that for the Antarctic temperature. The shutdown of the AMOC during the glacial termination causes a pronounced cooling, which delays warming in Greenland during the glacial termination. Only after a complete recovery of the AMOC does the Greenland temperature

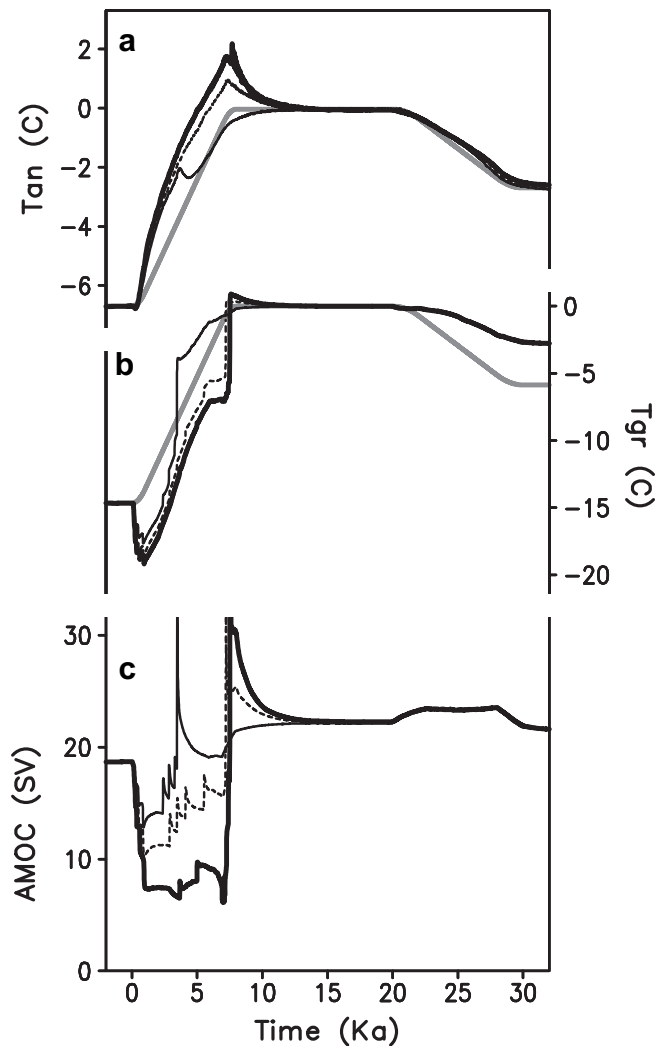


Fig. 7. Comparison of three experiments which differ only by the rate of freshwater flux during glacial termination: CI.20 (thin solid line), CI.15 (dashed line), CI.10 (thick solid line). (a) Antarctic temperature anomalies and (b) Greenland temperature anomalies compared to arbitrarily scaled GF (grey line). (c) Maximum of AMOC.

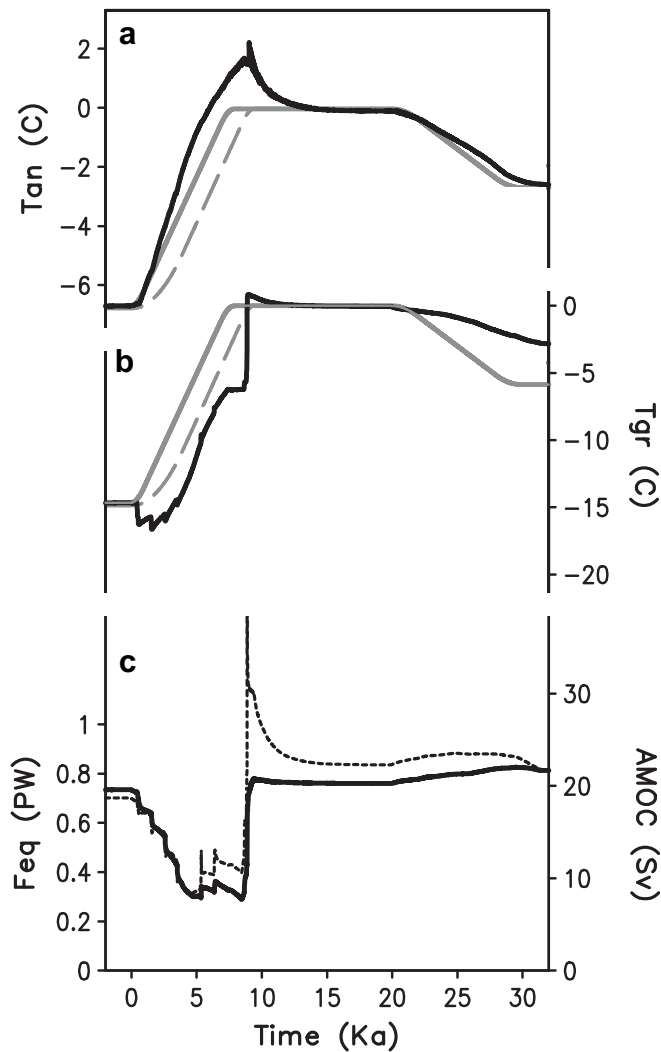


Fig. 8. Temporal evolution of annual mean climate characteristics in the experiment CI.20D where ice volume lags CO₂ during glacial termination by 2000 years. (a) Antarctic temperature anomalies and (b) Greenland temperature anomalies (black lines) compared to arbitrarily scaled CO₂ (solid grey line) and ice volume (dashed grey line). (c) Maximum of the AMOC (dashed line) and cross-equatorial northward oceanic heat transport (solid line).

reach its interglacial value, with a small overshoot. As a result, the Greenland temperature lags GF by 1000–2000 years depending on the methods used to determine leads and lags (Table 2). Thereby, if considering CO₂ concentration and global ice volume as the only climate forcings during glacial–interglacial–glacial transitions, one should conclude that the Antarctic temperature leads all climate forcings and the Greenland temperature lags all forcings, although the forcings are either applied only in the Northern Hemisphere (ice sheets and freshwater flux) or approximately hemispherically symmetric (CO₂).

Fig. 6 gives a global picture of the glacial–interglacial temperature change in experiment CI.20. It shows that at the midpoint of the deglaciation (i.e., at the model year 4000), the temperature in high latitudes of the Southern Hemisphere has risen by 80–90% of its glacial–interglacial difference, whilst in the Northern Hemisphere and, especially over the northern North Atlantic, the temperature remains close to its glacial value. This spatial-temporal dynamic of temperature change during the glacial termination is often referred to as the “early deglaciation” of the Southern Hemisphere and is sometimes interpreted as an indication of the

leading role of the Southern Hemisphere in the termination of the glacial cycles. Although the study of the mechanisms responsible for the glacial cycles is beyond the scope of this paper, it is important to note that in our experiment, the early warming of the Southern Hemisphere is solely explained by changes in the inter-hemispheric ocean heat transport forced by deglaciation of the Northern Hemisphere.

4.3. Sensitivity to the magnitude and the timing of freshwater forcing during glacial termination

Numerous experiments performed with climate models of different complexity demonstrate that the AMOC is sensitive to changes in freshwater flux into the Atlantic Ocean. However, it is also known that the models differ considerably in their sensitivity to changes in freshwater flux (e.g., Rahmstorf et al., 2005; Stouffer et al., 2006). On the other hand, it is also likely that although the maximum ice volume prior to the glacial terminations was similar during last several glacial cycles, the duration of the glacial terminations, and therefore the rate of meltwater discharge, differed considerably. Therefore, it is natural to explore the sensitivity of modeling results to the rate of freshwater discharge during glacial termination. To this end, we performed two additional experiments, CI.15 and CI.10, which are identical to CI.20 except that freshwater flux during the glacial terminations was similar to 0.15 and 0.1 Sv, respectively (Fig. 2c). These experiments could be considered as attempts to mimic models with a weaker sensitivity to the freshwater forcing or, alternatively, a longer duration of the glacial termination. In the latter case, it would also be natural to increase the duration of glacial termination to make it consistent with a weaker freshwater forcing. This option was tested and gives essentially the same results as the experiments where

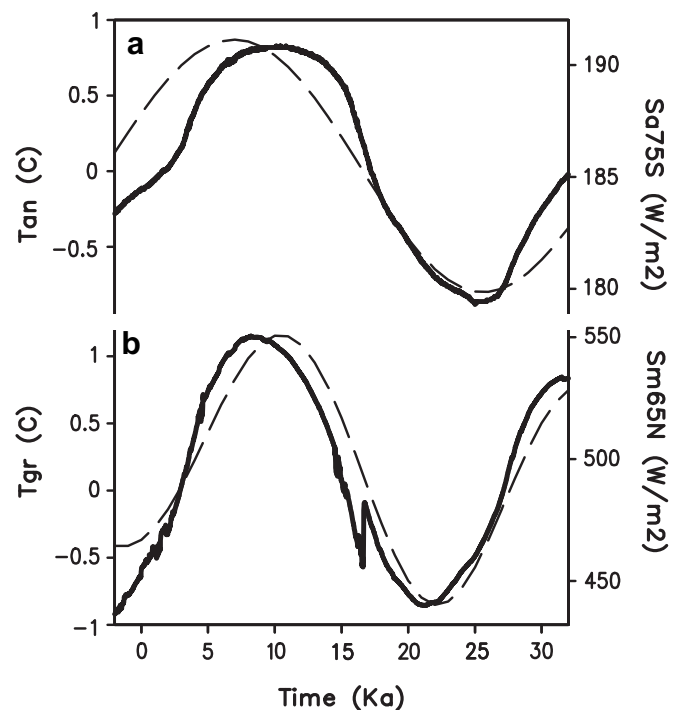


Fig. 9. Temporal evolution of annual mean climate characteristics in the experiment O where Earth's orbital parameters vary in time the same way as it was between 140 and 105 ka BP. All other boundary conditions are fixed and correspond to interglacial state. (a) Antarctic temperature anomalies and (b) Greenland temperature anomalies. Dashed lines in (a) represent annual mean insolation at 75°S and in (b) maximum summer insolation at 65°N.

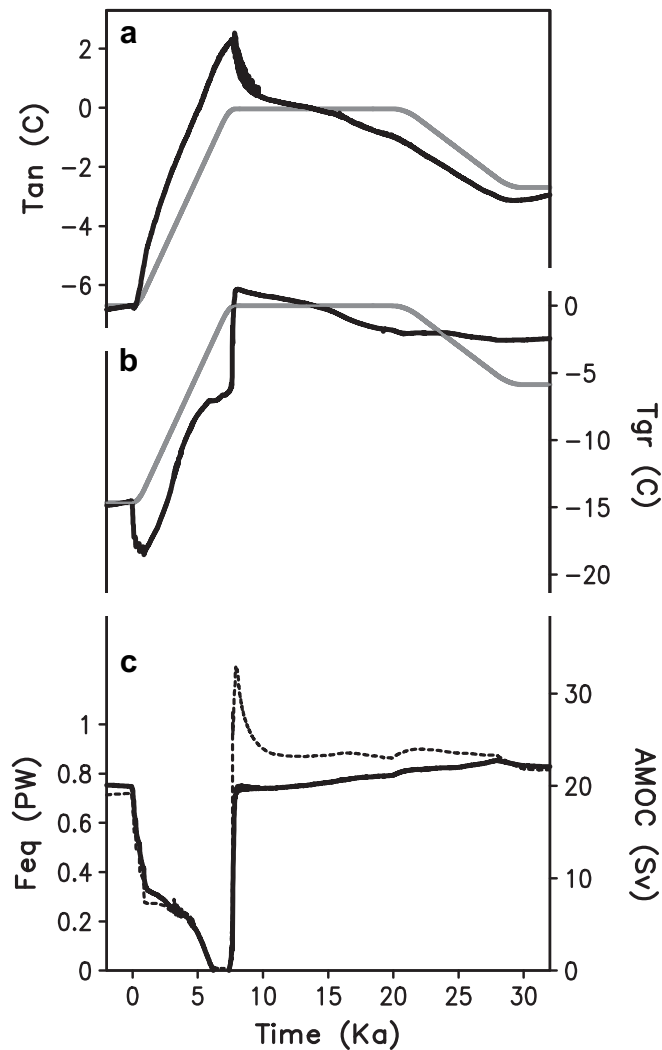


Fig. 10. The same as Fig. 5 but for the experiment CI0.20.

only the freshwater forcing was changed. Therefore, for the sake of simplicity and to make a comparison of different experiments more straightforward, here we present the simplest modeling setup, where experiments differ only by the magnitude of freshwater forcing during the glacial termination.

As is seen in Fig. 7, there is no qualitative difference between experiments CI.20 and CI.15, although a weakening of the AMOC is more modest in the latter and, as a result, the overshoot of Antarctic temperature is somewhat smaller. In both experiments, the AMOC recovers abruptly only at the end of the glacial termination. In both experiments, the Antarctic temperature leads and the Greenland temperature lags GF considerably. The situation is different in experiment CI.10, where the AMOC already recovered around the mid point of the glacial terminations, which causes an abrupt warming of the Greenland temperature and a temporary cooling of the Antarctic temperature resembling the so-called “Antarctic Cold Reversal” observed during Termination I. The abrupt increase of the AMOC around the midpoint of the termination in experiment CI.10 represents the transition from the “cold” (stadial) mode of the Atlantic thermohaline circulation to the “warm” (interstadial) mode and has the same mechanisms as the onset of Dansgaard–Oeschger events simulated by Ganopolski and Rahmstorf (2001). It is important to note, however, that unlike simulated abrupt climate changes by Ganopolski and Rahmstorf (2001), the transition from the “cold”

to the “warm” mode of the AMOC in experiment CI.10 is caused not by a change in freshwater flux, but by gradual global warming. As was argued by Ganopolski and Rahmstorf (2001) and supported by modeling results of Knorr and Lohmann (2007), as the climate warms, the “warm” mode of the AMOC becomes more stable and the “cold” mode becomes less stable. As experiment CI.10 shows, the transition from the “cold” to the “warm” mode of the Atlantic thermohaline circulation can occur as a result of global warming, even in the presence of sustained deglacial meltwater flux. If, however, this flux is sufficiently large, the recovery of the AMOC occurs only after the cessation of this flux. Comparison of these three experiments shows that climate change during the glacial termination is sensitive to the rate of deglaciation. Despite differences in temporal dynamics, the Antarctic temperature leads GF and hence the CO_2 concentration in all three experiments (Table 2).

In the previous experiments we assumed that the ice volume and CO_2 concentration have precisely the same temporal dynamics during the glacial termination, i.e., they start to decrease (rise) simultaneously and linearly till reaching the interglacial (glacial) level. The natural question is how crucial this assumption is for the simulated Antarctic temperature lead over CO_2 or, in other words, how robust are our findings, given existing uncertainties in the dating of the principal climate forcings during glacial terminations? Paleoclimate reconstructions for Termination I clearly show that sea level started to rise almost simultaneously with CO_2 concentration (Clark et al., 2004). However, using the midpoint of transition, or maximum correlation criteria, for the whole glacial termination, CO_2 leads ice volume by several thousand years. It is unknown whether a similar relationship took place for the earlier terminations, but to assess the robustness of our finding, we constructed an additional scenario (CI.20D) which differs from the original only through the ice volume dynamics during the glacial termination (Fig. 8). In this experiment, the ice volume starts to rise simultaneously with CO_2 concentration, but at the beginning it grows slower than CO_2 concentration and reaches its interglacial level 2000 years after CO_2 . As a result, the ice volume lags CO_2 by ca 2000 years in this experiment. As shown in Fig. 8, the temporal dynamics of the Antarctic and Greenland temperatures do not differ much from experiment CI.02, except that the Antarctic temperature at the beginning of the glacial termination rises somewhat slower and reaches its maximum (overshoot) simultaneously with the end of ice sheets melting. Still, irrespective of the criteria used, the Antarctic temperature leads CO_2 in experiment CI.20D by several hundred years and the Greenland temperature lags behind all forcings considerably. Therefore, the Antarctic lead over CO_2 is robust within a certain range of scenarios for the climate forcings.

4.4. The role of orbital forcing

Although it is believed that the main effect of orbital forcing on climate during glacial cycles is to drive the Northern Hemisphere ice sheets, even with the fixed ice sheets (e.g., for typical interglacial conditions), orbital forcing produces a pronounced effect on the annual mean temperature in the high latitudes of both hemispheres. As shown in Section 3, the Southern Hemisphere annual temperature is strongly affected by obliquity variations and, to a smaller extent, by the precessional cycle, which is explained by the fact that only obliquity affects annual mean insolation. The reason why we consider orbital forcing here in the rather broad context of glacial–interglacial transitions is that over essentially all recent glacial–interglacial terminations, orbital forcing has had a rather similar phase at the time of glacial termination and inception (e.g., Ruddiman, 2003; Huybers and Wunsch, 2005). Usually, glacial terminations have coincided with growing obliquity

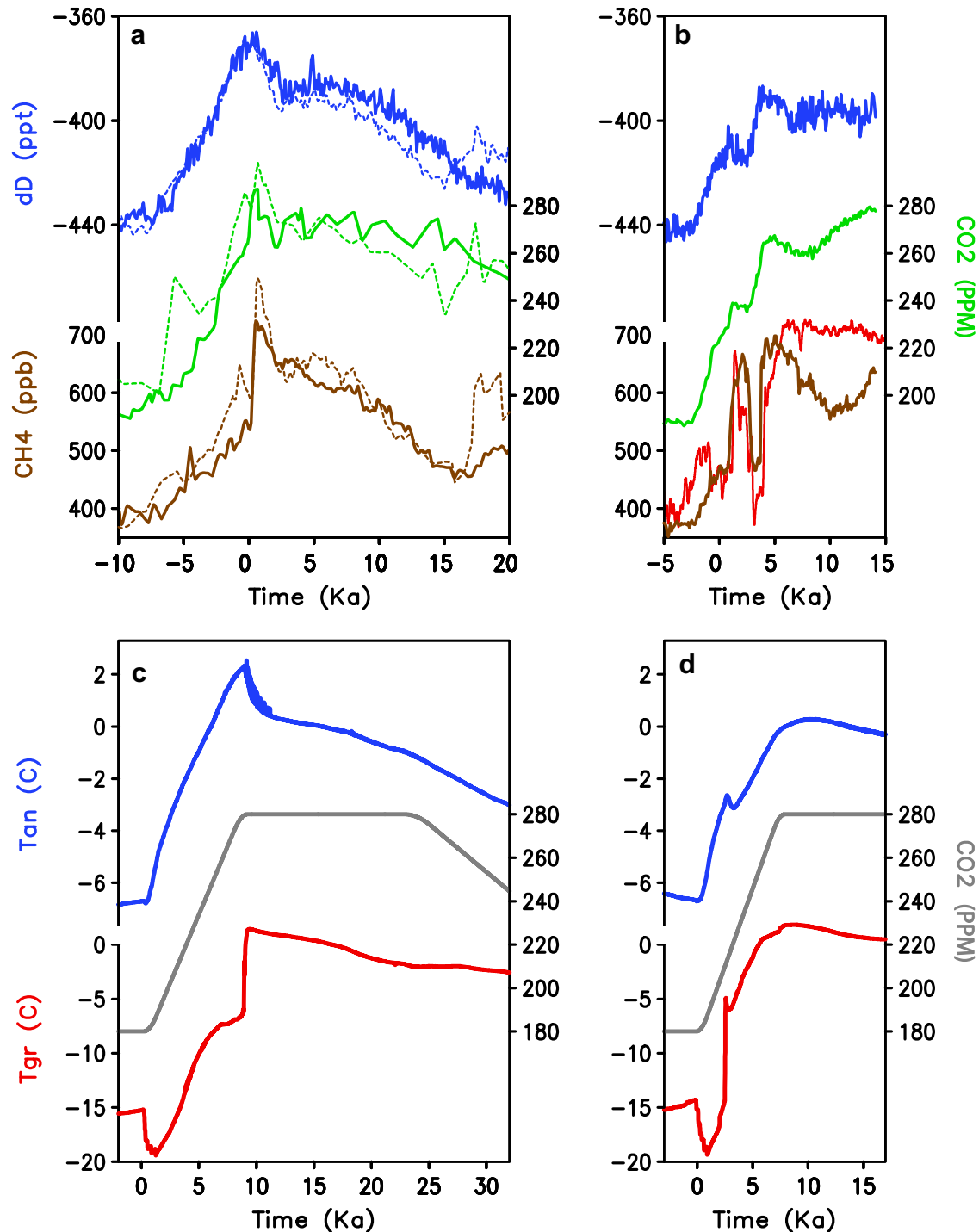


Fig. 11. Comparison of paleoclimate data (a) and (b) with modeling results (c) and (d). (a) Shows data for MIS5 (thick lines) and MIS7 (thin dashed lines), (b) for the Termination I and Holocene. (c) Shows Exp. CIO.20 and (d) Exp. CIO.10. Blue lines show annual mean Antarctic temperature anomalies and red lines Greenland temperature. Greenland temperature is absent in (a) and arbitrarily scaled in (b). In (a) and (b) green lines show atmospheric CO₂ concentration and brown lines show CH₄ concentration. In (c) and (d) grey lines show prescribed CO₂ concentration. Antarctic temperature, CO₂ and CH₄ are from EDC ice core on EDC3 time scale, Greenland temperature is from GISP-2 ice core.

and climatic precession (i.e., higher Northern Hemisphere summer insolation), whilst glacial inception occurred during periods of decreasing obliquity and climatic precession. This is, of course, not surprising if one accepts the Milankovitch theory, where both precession and obliquity play an important role in driving glacial cycles. On the other hand, a rather robust phase relationship between orbital forcing and glacial-interglacial transitions may contribute to a similarly robust phase relationship between

Antarctic temperature and CO₂, which is one of the central issue of the current study. We show below that this is indeed the case.

To better understand the transient response of the climate system to orbital forcing we performed an additional experiment, where we forced the climate with orbital variations only. In this experiment (hereafter referred to as experiment O) we kept interglacial boundary conditions, while the orbital parameters change in the same way as in reality, between 146 and 111 ka BP. As shown

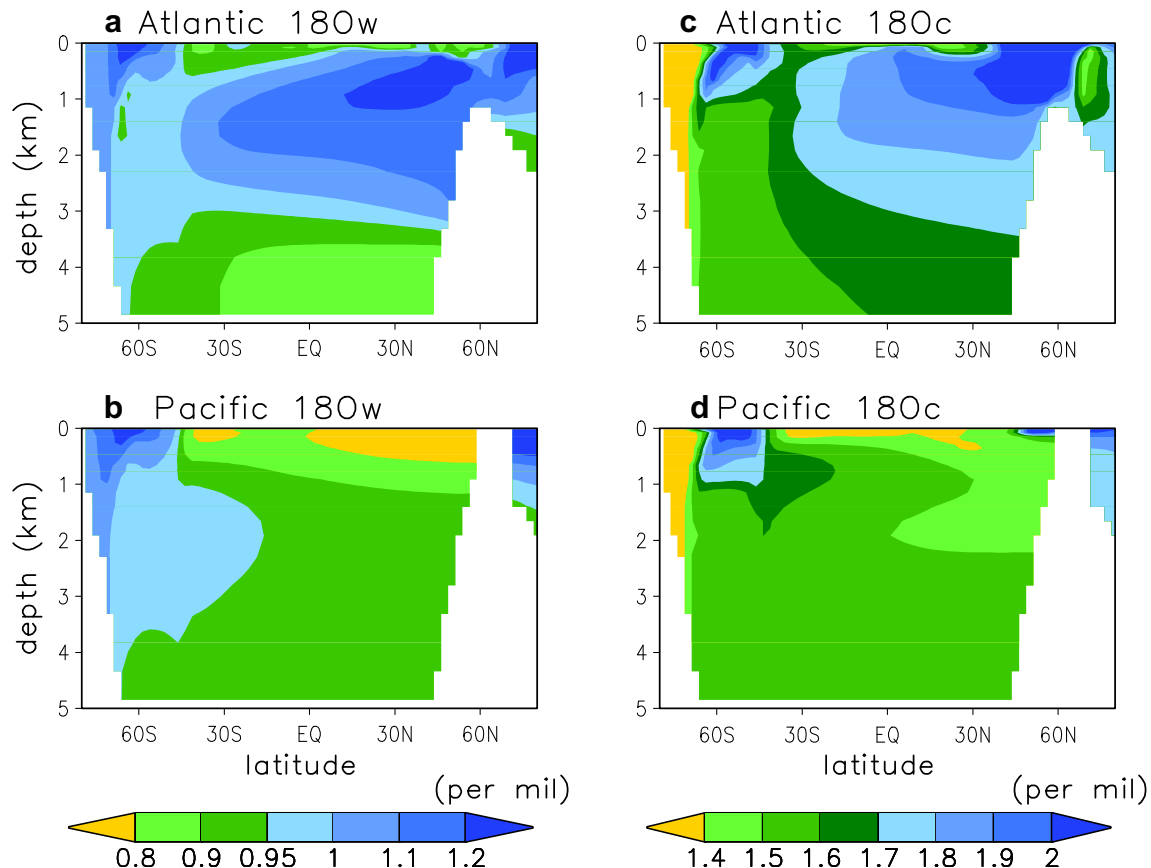


Fig. 12. Simulated zonally-averaged difference in $\delta^{18}O_w$ (a, b) and $\delta^{18}O_c$ (c, d) between the glacial and the interglacial climate states in the Atlantic (a, c) and Pacific (b, d).

in Fig. 9, both the Greenland and Antarctic temperatures respond appreciably and in a rather similar manner to orbital forcing. However, the Antarctic temperature follows obliquity variations (i.e., mean annual insolation) more closely, while Greenland temperature was more highly correlated with precessional variations (maximum summer insolation). The direct effect of orbital forcing in the high latitudes of Southern Hemisphere is strongly amplified by the sea ice-albedo feedback. Over the obliquity cycle, the annual mean area of sea ice in the Southern Hemisphere varies by about 10% and annual mean Antarctic temperature varies by about 2 °C. Thereby, the effect of orbital variations on Antarctic temperature is somewhat weaker, but still comparable with the effect of glacial–interglacial CO_2 variations. These results are fully consistent with the Timmermann et al. (2009) who used a much more detailed climate model of intermediate complexity.

To analyze the influence of orbital forcing on temperature changes, in combination with other forcings, we performed two additional experiments with realistic, time-dependent orbital forcing corresponding to the last two glacial–interglacial transitions. The first (experiment CIO.20) is identical to CIO.20 except that all orbital parameters during glacial–interglacial transition (i.e., from 0 to 35,000 model years) vary as during the interval of time between 146 and 111 ka BP. The second experiment, CIO.10, was intended to mimic Termination I and was identical to CIO.10 except that all orbital parameters vary as they varied during the last 20,000 years of Earth's history and that this experiment was run accordingly for 20,000 years only.

As is seen from comparison of Figs. 5 and 10, the main effect of orbital forcing is a pronounced cooling trend in the annual Antarctic temperature during the whole interglacial period. As a result, the Antarctic temperature drops by as much as 40% of its

maximum glacial–interglacial difference prior to the onset of the Northern Hemisphere glaciation and the beginning of the CO_2 decrease. With varying orbital forcing, the Antarctic temperature clearly leads CO_2 concentration both during the termination and the glacial inception, and its lead over the whole glacial–interglacial transition, as determined by the maximum correlation method, exceeds 2000 years (Table 2). A similar, but less pronounced, cooling trend is also seen in the Greenland temperature during the interglacial state.

4.5. Comparison with paleoclimate records

Although this study uses rather schematic forcing scenarios, which are not intended to accurately mimic any of the real glacial–interglacial transitions, a comparison of model simulations with paleoclimate data is nonetheless noteworthy and provides some insight into the mechanisms of climate change during real past glacial–interglacial transitions. Fig. 11 shows a comparison of paleoclimate records for two earlier glacial–interglacial transitions (Terminations II/MIS5 and IV/MIS9) and the last glacial–interglacial transitions with the results of experiments CIO.20 and CIO.10, respectively. For the earlier terminations, a detailed Greenland temperature record does not exist and we used methane concentration as a proxy for the Greenland temperature – justified, at least to some extent, by a strong similarity between the Greenland temperature and the methane concentration during the last glacial cycle (Fig. 11b). Paleoclimate records of the MIS5 and MIS9 are matched in time by the timing of abrupt increase in CH_4 concentration which also coincides with the maximum of Antarctic temperature and CO_2 concentration. The similarity between temporal dynamics of the Antarctic temperature, CO_2 and CH_4

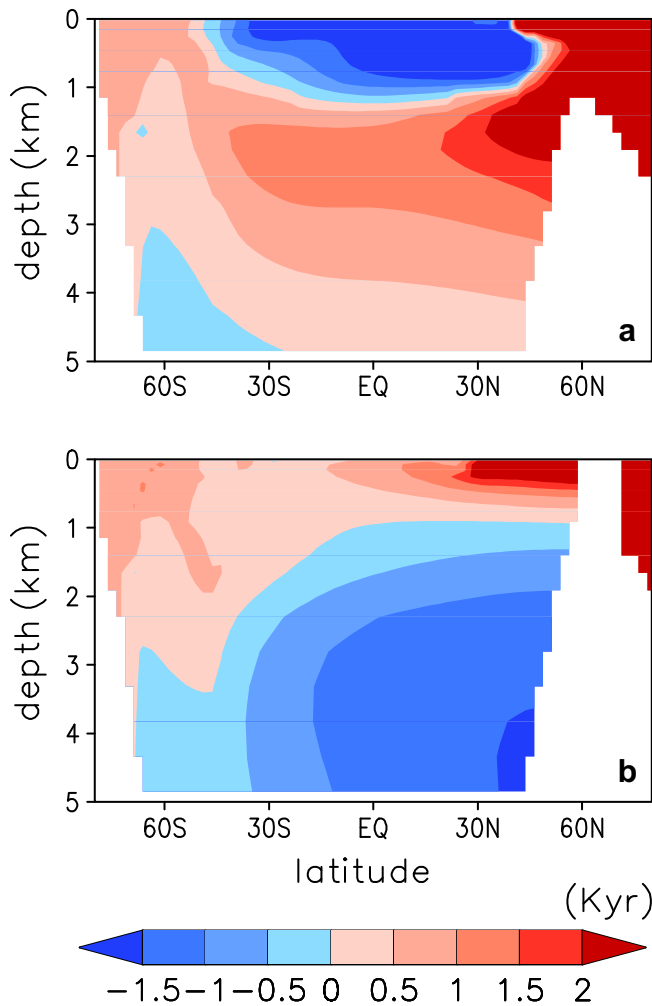


Fig. 13. Time differences (in Kyr) between midpoint of glacial–interglacial transition of $\delta^{18}O_w$ and midpoint of GF in the Atlantic (a) and Pacific (b). Positive values mean that $\delta^{18}O_w$ leads GF.

concentrations during these two glacial–interglacial transitions are rather indicative for the existence of common mechanisms. It is noteworthy that the dynamics of the termination during MIS7 are rather similar (not shown), but no stable interglacial state is seen in the latter case. In particular, all three earlier terminations are characterized by simultaneous “overshoots” in Antarctic temperature, CO_2 and CH_4 concentrations occurring at the end of terminations. To the contrary, during the Termination I, the CH_4 concentration increases abruptly at the early stage of the termination, simultaneous with the local maximum in the Antarctic temperature, which is well below the interglacial value of the Antarctic temperature.

While one should not expect one-to-one correspondence between paleo data and model simulations in light of rather schematic forcing scenarios and obvious limitations of the model used for this study, there are a number of important similarities between the model results and the paleo data. In particular, a pronounced overshoot of the Antarctic temperature at the end of Terminations II and IV and a cooling trend during the MIS5 and 9 interglacials seen in paleoclimate records are reproduced in experiment CIO.20. Similar to the simulated Greenland temperature, the methane concentration rises slowly during most of Terminations II and IV, and then increases abruptly at the end of the glacial–interglacial transition, at the time when Antarctic temperature reaches its maximum.

Similarity between Termination I and CIO.10 is less evident because our model does not simulate the abrupt Younger Dryas event. More realistic simulation of Termination I would require a more sophisticated freshwater scenario but this is beyond the scope of this schematic study. However, the model and paleo data agree in an early recovery of the AMOC, which is associated with the temporal reversal of the Antarctic temperature resembling an “Antarctic Cold Reversal” at around 14 ka BP. Besides, both model and data do not show a strong Antarctic temperature overshoot at the end of the last termination and both show a clear cooling trend of the Antarctic and Greenland temperatures during the interglacial (Holocene). Through the design of model experiments, in our simulation, this cooling trend is solely attributed to orbital forcing, primarily the decrease of obliquity which causes a decrease in annual insolation at high latitudes in both hemispheres. It is noteworthy that the maximum Antarctic temperature at the onset of the interglacial state is about $2^\circ C$ higher in experiment CIO.20 as compared to CIO.10. A similar difference in temperature is seen in the reconstructed Antarctic temperature between Eemian interglacial and Holocene. This difference is often interpreted as an indication that the Eemian interglacial was globally much warmer than the Holocene. In fact, at least in our experiments, considerably warmer temperatures in CIO.20 are restricted to the Antarctic realm, while for the rest of the world, the difference in annual temperatures between these two interglacials is much smaller.

Our results suggest that the major differences in temperature evolution, both in Greenland and Antarctica, during the last and previous three terminations can be explained by the difference in the timing of recovering the present-day mode of the AMOC. Namely, in experiment CIO.20, which we consider as an analog for the Terminations II and IV, the late recovery of the AMOC leads to a strong overshoot of the Antarctic temperature and a strong

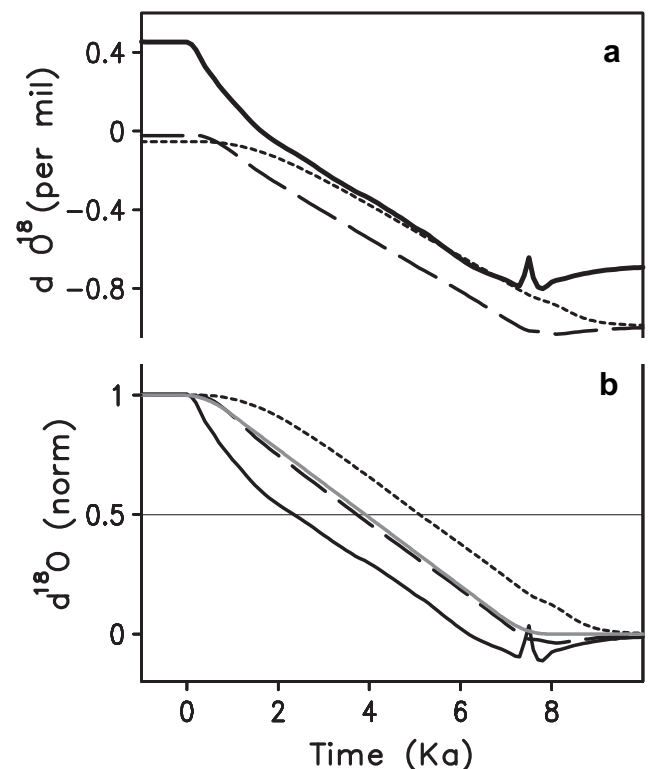


Fig. 14. Temporal evolution of $\delta^{18}O_w$ during glacial termination in the deep Atlantic (30°N, 3000 m depth; solid line) and the deep Pacific (30°N, 3000 m depth; dashed line). (a) Absolute values; and (b) values normalized by the glacial–interglacial differences. Grey line shows normalized GF.

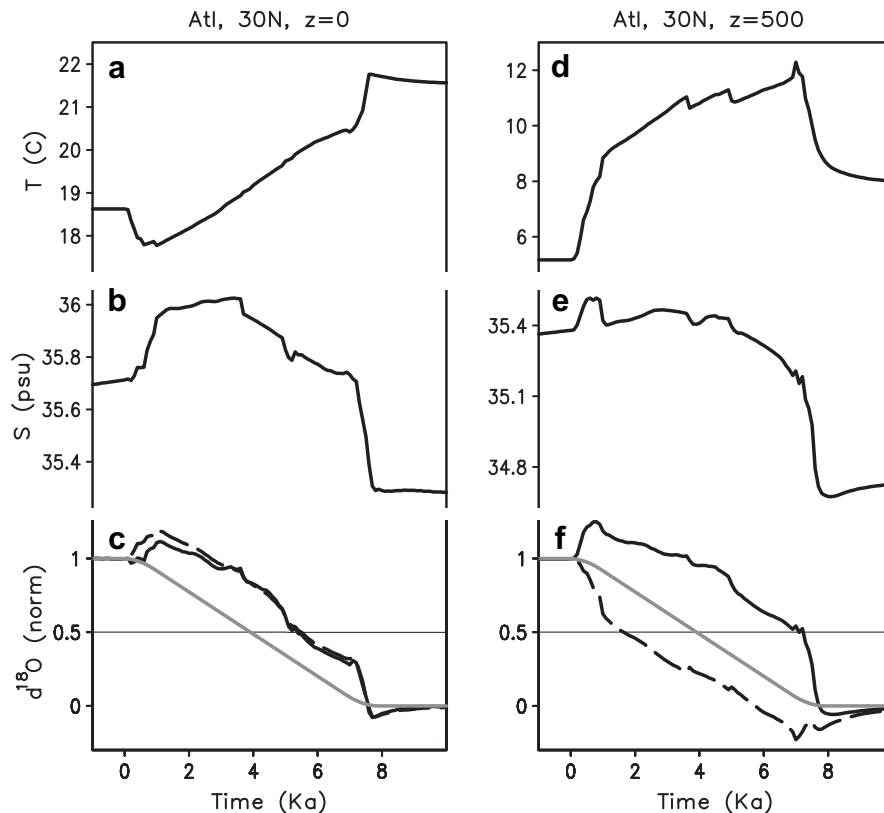


Fig. 15. Temporal evolution of temperature (a, d), salinity (b, e), $\delta^{18}\text{O}_w$ (solid) and $\delta^{18}\text{O}_c$ (dashed) (c, f) during the glacial termination in the subtropical Atlantic (30°N, mixed layer, left panel) and (30°N, 500 m depth, right panel). Grey lines show normalized GF.

cooling trend during the whole interglacial. In experiment CIO.10 (an analog for the last termination), early recovery of the AMOC causes the Antarctic cold reversal, but not a strong temperature overshoot at the onset of the interglacial. As a result, the Antarctic cooling trend during interglacial is much less pronounced in the latter case. Available paleo data provide no clear evidence for B/A – YD type of climate oscillations during Terminations II–IV. This is consistent with a record from the Iberian margin (Martrat et al., 2007), which indicates that establishment of the interglacial mode of the AMOC during Termination II occurred at the end of the glacial–interglacial transitions, while for Termination I, the situation was different and characterized by the reestablishment of the deep Atlantic ventilation at an early stage of the deglaciation. All of these facts support the notion that our experiment CIO.20 is representative for the penultimate and, likely, for several early terminations.

5. $\delta^{18}\text{O}$ response in the oceans to the glacial termination

In this section, we make use of the fact that the CLIMBER-2 model incorporates the description of the oxygen-18 cycle to analyze the temporal dynamics of this widely used paleoclimate tracer in the oceans during glacial–interglacial transitions. It is well-known that the relative ^{18}O concentration of the calcite of foraminifera shells retrieved in marine sediment cores (hereafter $\delta^{18}\text{O}_c$) is controlled by local temperature, global ice volume changes and by changes in the global hydrological cycle. In paleoclimatology, two classical approaches are used for reconstructing past global ice volume and salinity.

The benthic $\delta^{18}\text{O}_c$ in deep sediment cores is usually considered as a proxy for global ice volume and hence assumed to have similar temporal dynamics in different locations. Indeed, compiling

benthic $\delta^{18}\text{O}_c$ in deep ocean locations is classically thought to smooth the hydrological cycle signal, leaving the global ice volume and the local temperature. Assuming that deep ocean temperature is fairly homogeneous and close to the freezing point during glacial times leaves only global ice volume as a meaningful signal. This in turn justifies the use of benthic $\delta^{18}\text{O}_c$ for synchronization of different marine records. Here we show that this series of assumptions is not held – at least during glacial–interglacial transitions – and that synchronization of different records via $\delta^{18}\text{O}_c$ can lead to large absolute and relative dating errors.

The planktic $\delta^{18}\text{O}_c$ of foraminifera shells integrate a more local signal not only with the global ice volume and the local temperature, but also with local and global changes in the hydrological cycle. Knowing the global ice volume and being able to estimate the local temperature (by means of foraminiferal species assemblages, Mg/Ca, Alkenones, etc., techniques) leaves only the $\delta^{18}\text{O}_w$ (relative ^{18}O abundance in sea water) as a meaningful signal. Based on the present-day measured spatial relationship between salinity and $\delta^{18}\text{O}_w$, one can estimate the changes in local salinity, a target of great value for both data–model comparisons and physical understanding of the dynamics of past ocean circulation. Such a method (Duplessy et al., 1991) relies on the fact that the present-day spatial $\delta^{18}\text{O}_w$ – salinity relationship is held through time, which is yet unknown. As we simulate both salinity and $\delta^{18}\text{O}_w$, we can address this question for the glacial – interglacial cycles. We show hereafter, that the variations of $\delta^{18}\text{O}_w$ and salinity are not coeval, and that the local spatial $\delta^{18}\text{O}_w$ – salinity relationship is not maintained through time.

Simulation with the oxygen-18 cycle model discussed below was performed using the same forcings as in experiment CIO.20, but was restricted to the glacial termination phase only. The reason for that is that oxygen-18 cycle model used in this study does not explicitly include ice sheets. This model limitation can be

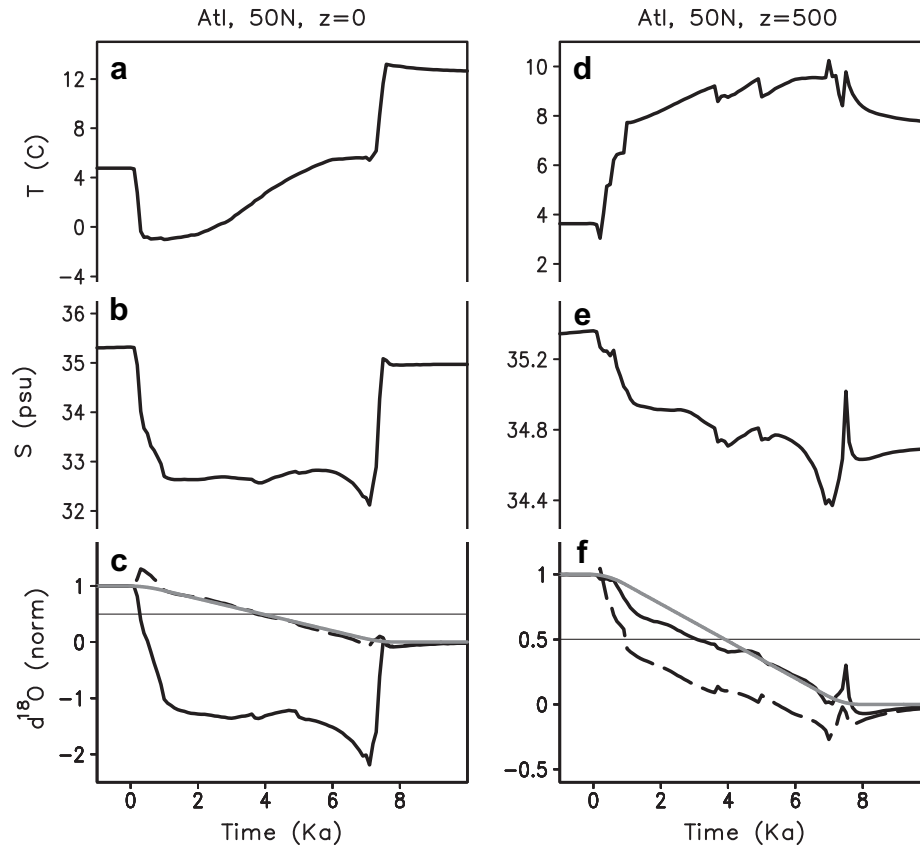


Fig. 16. Temporal evolution of temperature (a, d), salinity (b, e), $\delta^{18}\text{O}_w$ (solid) and $\delta^{18}\text{O}_c$ (dashed) (c, f) during the glacial termination in the midlatitude Atlantic (50°N, mixed layer, left panel) and (50°N, 500 m depth, right panel). Grey lines show normalized GF.

circumvented for the deglaciation phase if we assume that most of anomalous ^{18}O flux into the ocean during deglaciation was associated with meltwater from the Northern Hemisphere ice sheets. Similar to Roche et al. (2004b), we prescribed anomalous ^{18}O flux consistent with anomalous freshwater flux and applied it to the same area assuming isotopic composition of glacial meltwater of -30‰ . During periods of ice sheet growth, the situation is not symmetric because anomalous freshwater flux originates from net evaporation from different regions of the ocean and simulation of ^{18}O in this case requires a much more complex modeling approach.

5.1. Deep ocean response

Figs. 12a–d show simulated $\delta^{18}\text{O}_w$ and $\delta^{18}\text{O}_c$ differences between the glacial and interglacial states in the Atlantic and the Pacific obtained in experiments with the oxygen-18 cycle model. The globally averaged change in $\delta^{18}\text{O}_w$ is about 0.95‰ , which corresponds to the implied 100 m sea level change between the glacial and the interglacial climate states. Simulated changes in $\delta^{18}\text{O}_w$ are rather uniform in the deep Pacific in our model, while the structure is more complex in the Atlantic. In the upper part of the Atlantic, differences in $\delta^{18}\text{O}_w$ are higher than the globally average, while in the deep Atlantic, the $\delta^{18}\text{O}_w$ increase is smaller than the global average. It is noteworthy that these changes are opposite to what one would expect from a simple $\delta^{18}\text{O}_w$ – salinity relationship. Indeed, in our simulations, deep Atlantic salinity increases in the glacial state more than the averaged increase (1‰) whilst NADW water masses become relatively fresher (see Brovkin et al. (2007) for details). The explanation of this apparent contradiction lies in the fact that increased salinity of the glacial AABW is related to enhanced sea ice formation and brine rejection around Antarctica,

a process which increases salinity of deep water masses but barely modifies their $\delta^{18}\text{O}_w$. As a result, $\delta^{18}\text{O}_w$ in the AABW remains lower than that in the glacial NADW and a substitution of the latter by the former in the deep Atlantic under glacial conditions leads to a relative decrease in $\delta^{18}\text{O}_w$ here. At the same time, a southward shift of NADW formation area leads to a relative increase of $\delta^{18}\text{O}_w$ in the NADW during the glacial state.

Glacial–interglacial temperature changes explain more than one third of the $\delta^{18}\text{O}_c$ change (Figs. 12c,d) in our simulations. In the current version of the CLIMBER-2 model, the deep ocean glacial temperature is lower than that of the interglacial by 2–3 °C (Brovkin et al., 2007), which is in a better agreement with paleoceanographic data than it was in the earlier version of the CLIMBER-2 model used by Roche et al. (2004a). As a result, the $\delta^{18}\text{O}_c$ distribution in the deep ocean is also more consistent with the data. In particular, the glacial–interglacial change of $\delta^{18}\text{O}_c$ in the deep Atlantic is within the range 1.6–1.8 ‰, and 1.5–1.6 ‰ in the deep Pacific.

Fig. 13 shows the timing of the midpoint of the glacial–interglacial transition in $\delta^{18}\text{O}_w$ in the Atlantic and Pacific, as compared to the real timing of the midpoint of GF transition. As is seen in the figures, the midpoint in the $\delta^{18}\text{O}_w$ transition is reached in the deep Atlantic by up to 2000 years earlier and in the Pacific by more than 1000 years later than the midpoint of the GF. The delay in response of the deep Pacific is obvious and is explained by the millennial time scale of the propagation of the meltwater signal from the North Atlantic surface into the deep Pacific. The cause of the apparent lead in the North Atlantic is related to a stronger initial freshening of the Northern Atlantic, as compared to that implied by the globally averaged salinity changes during the glacial–interglacial transition. As a result, the deep Atlantic $\delta^{18}\text{O}_w$ leads that of the deep Pacific by up to 3000 years. Interestingly enough, Skinner and Shackleton (2005) found a similar time lag (ca

4000 years) of the deep Pacific $\delta^{18}\text{O}$ record, as compared that of the deep Atlantic. They correctly noted that this lag is too large to be solely attributed to the long resident time of the deep Pacific water masses and proposed that a part of this lag is attributed to different rates of deglacial warming in the deep Atlantic and in the Pacific. While it is likely that the latter factor also contributed to the Atlantic lead, our results demonstrate that a considerably portion of the observed 4000 year time lag of the Pacific compared to the Atlantic can be explained by $\delta^{18}\text{O}$ in sea water, i.e., without an additional temperature effect. Thus, irrespective of the role of deep ocean temperature changes, our results support the Skinner and Shackleton (2005) notion that the use of $\delta^{18}\text{O}_c$ for the synchronization of paleo-oceanographic records from different oceans could lead to a very large dating error, comparable with the time scale of the glacial–interglacial transitions. Additionally, the lead–lag relationship between the deep Atlantic and the deep Pacific is not constant through time as is shown in Fig. 14, where the time evolution of the $\delta^{18}\text{O}_w$ is compared for both oceans. The maximum lag of the deep Pacific is found, in our model, around the mid-transition point for our scenario. Though the exact timing will depend on the subtlety of the scenario used for the deglaciation, the ~2500 years needed by the deep Pacific to “catch up” with the deep Atlantic signal is probably robust, being linked to the mixing time scale of the world ocean.

5.2. Upper ocean response

The temporal evolution of $\delta^{18}\text{O}$ in the upper ocean is even more complicated. As is shown in Fig. 13, $\delta^{18}\text{O}_w$ in most of the surface Atlantic lags the GF considerably, except for in the high latitude Atlantic. The reason for this, as seen from Fig. 15, is that the AMOC shutdown during the glacial termination leads to an increase of salinity in the tropics, which offsets the effect of the global salinity decrease during deglaciation. Since the dynamics of surface salinity and temperature are similar, the response of $\delta^{18}\text{O}_w$ and $\delta^{18}\text{O}_c$ are similar as well (but do not follow the present-day local $\delta^{18}\text{O}_w$ – salinity relationship, see hereafter). This is not the case for the intermediate depths in the Atlantic. There, changes in salinity and $\delta^{18}\text{O}_w$ are essentially the same as at the surface, but a strong subsurface warming leads to a very different temporal evolution of $\delta^{18}\text{O}_w$ and $\delta^{18}\text{O}_c$. The former, as at the surface, lags the GF whilst the latter leads the GF. Hence results of our simulations indicate that in the subtropical North Atlantic, the planktic $\delta^{18}\text{O}$ signal (both in sea water and calcite) lags the ice volume by several thousand years, the benthic signal leads the global ice volume by up to several thousand years, and the subsurface signal (for example, from the deep dwelling planktic species) can both lead and lag the global ice volume by several thousand years depending on the sign and the magnitude of subsurface temperature response to a weakening or complete shutdown of the AMOC. In the high latitude Atlantic, the pattern is quite different for both the salinity and $\delta^{18}\text{O}_w$, due to the strong freshening of the surface from the large freshwater flux during the deglaciation, as shown in Fig. 16. The evolutions of temperature and of salinity (and $\delta^{18}\text{O}_w$) are closely related to a strong decrease at the beginning of the deglaciation and an increase at the end. This leads to a simulated $\delta^{18}\text{O}_c$ almost perfectly in phase with the GF, because the temperature and $\delta^{18}\text{O}_w$ variations compensate each other almost perfectly (as can be found during Heinrich events, see Roche and Paillard, 2005). At intermediate depths, the ocean experiences a warming and a freshening throughout the deglaciation. The temperature variations therefore do not compensate for the $\delta^{18}\text{O}_w$ evolution there, causing $\delta^{18}\text{O}_c$ to considerably lead the GF – by more than 2000 years.

As for the evolution of the $\delta^{18}\text{O}_w$ – salinity relationship on glacial – interglacial timescales, we show the evolution of the slope of the local spatial $\delta^{18}\text{O}_w$ – salinity relationship on Fig. 17. At high

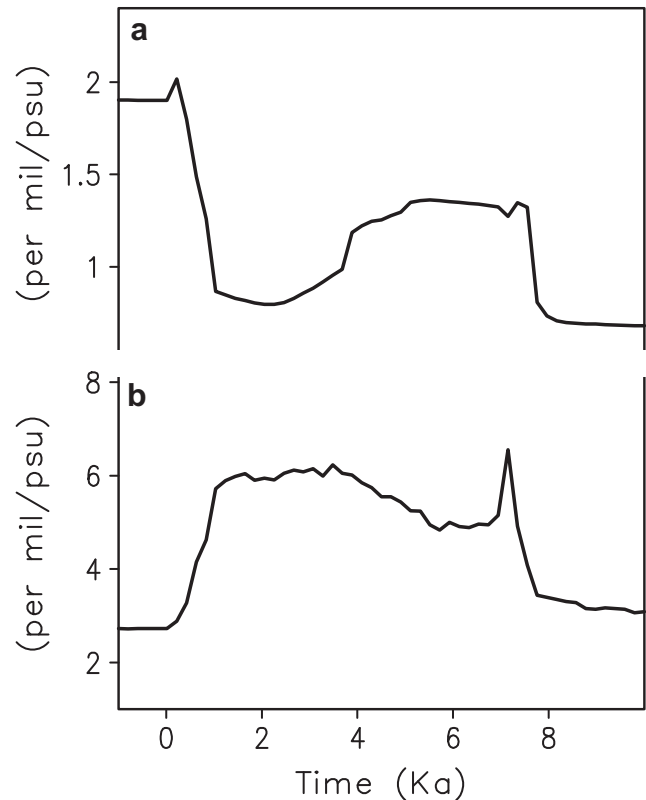


Fig. 17. Temporal evolution of the local $\delta^{18}\text{O}_w$ – salinity relationship in the surface Atlantic at 30°N (a) and 50°N (b).

latitude (50°N), the slope decreases during the deglaciation due to the input of low $\delta^{18}\text{O}_w$ deglacial meltwater fluxes and the disruption of the AMOC. The slope then increases when the interglacial circulation is established, returning to present-day like values. The large variability of the local spatial $\delta^{18}\text{O}_w$ – salinity slope during the deglaciation (by a factor of two) would imply errors of several per mil on the reconstructed salinities, if it were considered invariant. This is also true at lower latitude (30°N), where the slope of the spatial $\delta^{18}\text{O}_w$ – salinity relationship increases by a factor of two in our model during the deglaciation, due to a relative increase in $\delta^{18}\text{O}_w$ with respect to salinity. While the $\delta^{18}\text{O}_w$ – salinity relationship is known to be less reliable closer to the equator where the local hydrological cycle may have a strong impact on the $\delta^{18}\text{O}_w$ but not on salinity, this temporal evolution of the local spatial slope seems to be quite robust in the model for the glacial period and the deglaciation (but, as expected, with a lower correlation coefficient for the interglacial). This certainly should be investigated further, but already shows that great caution is needed when using $\delta^{18}\text{O}_w$ – salinity relationships to infer past salinities.

6. Discussion and conclusions

Results of our simulations with generic scenarios for glacial–interglacial transitions show that the observed millennial lead of the Antarctic temperature over CO_2 concentration can be explained by the fact that, although CO_2 concentration variation during glacial cycles is the most important factor affecting the Antarctic temperature, the other factors, such as changes in the oceanic heat transport and orbital forcing, also play significant roles and they have very different temporal dynamics compared to the CO_2 concentration. Our experiments, although rather schematic, reproduce a number of important features seen in the paleoclimate

records, as well as the correct phase relationships between climate forcings and temperatures. Our results clearly show that observed changes can only be successfully reproduced if all major climate forcings and processes are accounted for. As a result, a simple interpretation of leads and lags as an indicator of causal relationships in the climate system can lead to a false conclusion. In summary,

1. Our results demonstrate that any attempt to use the observed lead of the Antarctic temperature over CO₂ concentration to challenge the major role of greenhouse gases in driving climate change is baseless. Indeed, in our simulations CO₂ forcing alone explains half of the glacial–interglacial temperature variations in Antarctica and, nonetheless, the Antarctic temperature leads the CO₂ concentration significantly.
2. Our results illustrate a possible problem with using leads and lags to establish a causal relationship between different processes in the climate system. Indeed, if one would consider CO₂ concentration and the global ice volume as the sole climate forcings during the glacial–interglacial transitions, then one would come to a paradoxical conclusion that the Antarctic temperature led all of its forcings. This apparent paradox is resolved by taking into account the freshwater flux which, as the temporal derivative of the global ice volume, has totally different temporal dynamics compared with the global ice volume. Such a simple example shows that the leads and lags between different paleoclimate proxies do not provide direct information about causal relationships in the climate system.
3. Our results show that the high correlation between the Antarctic temperature and CO₂ concentration and the phase lead of the former cannot be considered as evidence for the leading role of the Southern Hemisphere in driving the glacial cycles. Indeed, in our simulations, the Southern Hemisphere temperature lead arises from the response to the Northern Hemisphere forcing (ice sheets), global CO₂ and local orbital forcing.
4. Our results demonstrate that a stronger Antarctic warming at the beginning of several previous interglacials, as compared to the Holocene, may be explained by the temperature overshoot associated with the late recovery of the AMOC. Hence, the qualitative difference between different terminations may result from a modest difference in the rates of the deglaciations. At the same time, a pronounced Antarctic cooling trend seen during most interglacials can be explained by the orbital forcing, primarily by decreasing obliquity.
5. Our simulations of $\delta^{18}\text{O}_w$ in the ocean during glacial terminations show that the temporal evolution of this tracer can considerably deviate from the global ice volume. In particular, in the deep Atlantic, $\delta^{18}\text{O}_w$ leads the global ice volume while in the Pacific it considerably lags the global ice volume. Temperature effect on $\delta^{18}\text{O}_c$ additionally complicates its temporal dynamics. As a result, the use of $\delta^{18}\text{O}$ for the synchronization of different paleoclimate records introduces large relative dating errors, of up to several thousand years in our simplified experiments.
6. Analysis of the temporal evolution of the local $\delta^{18}\text{O}_w$ – salinity relationship in our model shows that, the local spatial slope between these two tracers is not invariant on glacial–interglacial timescales and that great caution is needed when interpreting past $\delta^{18}\text{O}_w$ levels as a proxy for past salinities.

The overall conclusion of our work is that the ultimate understanding of past climate changes will only be possible using paleoclimate records in conjunction with comprehensive Earth system models, which simulate not only climate characteristics but also the paleoclimate proxies themselves.

References

- Alley, R.B., Brook, E.J., Anandakrishnan, S., 2002. A northern lead in the orbital band: north–south phasing of Ice-Age events. *Quaternary Science Reviews* 21, 431–441.
- Blunier, T., Chappellaz, J., Schwander, J., Dällenbach, A., Stauffer, B., Stocker, T., Raynaud, D., Jouzel, J., Clausen, H.B., Hammer, C.U., Johnsen, S.J., 1998. Asynchrony of Antarctic and Greenland climate change during the last glacial period. *Nature* 394, 739–743.
- Broecker, W.S., 2003. Does the trigger for abrupt climate change reside in the ocean or in the atmosphere? *Science* 300, 1519–1522.
- Brovkin, V., Bendtsen, J., Claussen, M., Ganopolski, A., Kubatzki, C., Petoukhov, V., Andreev, A., 2002. Carbon cycle, vegetation and climate dynamics in the Holocene: experiments with the CLIMBER-2 model. *Global Biogeochemical Cycles* 16, 86.1–86.20. doi:10.1029/2001GB001662.
- Brovkin, V., Ganopolski, A., Archer, D., Rahmstorf, S., 2007. Lowering of glacial atmospheric CO₂ in response to changes in oceanic circulation and marine biogeochemistry. *Paleoceanography*, 22, PA4202. doi:10.1029/2006PA001380.
- Caillon, N., Severinghaus, J.P., Jouzel, J., Barnola, J.-M., Kang, J., Lipenkov, V.Y., 2003. Timing of atmospheric CO₂ and Antarctic temperature changes across termination III. *Science* 299, 1728–1731.
- Clark, P.U., McCabe, A.M., Mix, A.C., Weaver, A.J., 2004. Rapid rise of sea level 19,000 years ago and its global implications. *Science* 304, 1141–1144.
- Claussen, M., Fohlmeister, J., Ganopolski, A., Brovkin, V., 2006. Vegetation dynamics amplifies precessional forcing. *Geophysical Research Letters* 33, L09709. doi:10.1029/2006GL026111.
- Crowley, T.J., 1992. North Atlantic deep water cools the Southern Hemisphere. *Paleoceanography* 7, 489–497.
- Duplessy, J.-C., Labeyrie, L., Juillet-Leclerc, A., Maitre, F., Duprat, J., Sarnthein, M., 1991. Surface salinity reconstruction of the North Atlantic Ocean during the last glacial maximum. *Oceanologica Acta* 14, 311–324.
- EPICA Community Members, 2006. Interhemispheric coupling of millennial scale variability during the last glacial. *Nature* 444, 195–198.
- Fischer, H., Wahlen, M., Smith, J., Mastroianni, D., Deck, B., 1999. Ice core records of Atmospheric CO₂ around the last three glacial terminations. *Science* 283, 1712–1714.
- Ganopolski, A., Rahmstorf, S., Petoukhov, V., Claussen, M., 1998. Simulation of modern and glacial climates with a coupled global model of intermediate complexity. *Nature* 391, 351–356.
- Ganopolski, A., 2003. Glacial integrative modelling. *Philosophical Transactions of the Royal Society A* 361, 1871–1884.
- Ganopolski, A., Rahmstorf, S., 2001. Rapid changes of glacial climate simulated in a coupled climate model. *Nature* 409, 153–158.
- Ganopolski, A., Petoukhov, V., Rahmstorf, S., Brovkin, V., Claussen, M., Eliseev, A., Kubatzki, C., 2001. CLIMBER-2: a climate system model of intermediate complexity. Part II: model sensitivity. *Climate Dynamics* 17, 735–751.
- Harvey, L.D., 1989. Milankovitch forcing, vegetation feedback and North Atlantic deep water formation. *Journal of Climate* 2, 800–815.
- Hewitt, C.D., Mitchell, J.F.B., 1997. Radiative forcing and response of a GCM to ice age boundary conditions: cloud feedback and climate sensitivity. *Climate Dynamics* 13, 821–834.
- Huybers, P., Denton, G., 2008. Antarctic temperature at orbital timescales controlled by local summer duration. *Nature Geoscience* 1, 787–792.
- Huybers, P., Wunsch, C., 2005. Obliquity pacing of the late Pleistocene glacial terminations. *Nature* 443, 491–494.
- Jouzel, J., Vimeux, F., Caillon, N., Delayue, G., Hoffmann, G., Masson-Delmotte, V., Parrenin, F., 2003. Magnitude of isotope/temperature scaling for interpretation of central Antarctic ice cores. *Journal Geophysical Research – Atmosphere* 108, D18. doi:10.1029/2002JD002677.
- Knorr, G., Lohmann, G., 2007. Rapid transitions in the Atlantic thermohaline circulation triggered by global warming and meltwater during the last deglaciation. *Geochemistry Geophysics Geosystems* 8, Q12006. doi:10.1029/2007GC001604.
- Martrat, B., Grimalt, J.O., Shackleton, N.J., de Abreu, L., Hutterli, M.A., Stocker, T.F., 2007. Four climate cycles of recurring deep and surface water destabilizations on the Iberian Margin. *Science* 317, 502–507. doi:10.1126/science.1139994.
- Monnin, E., Indermühle, A., Dällenbach, A., Flückiger, J., Stauffer, B., Stocker, T.F., Raynaud, D., Barnola, J.-M., 2001. Atmospheric CO₂ concentrations over the last glacial termination. *Science* 291, 112–114.
- Petoukhov, V., Ganopolski, A., Brovkin, V., Claussen, M., Eliseev, A., Kubatzki, C., Rahmstorf, S., 2000. CLIMBER-2: a climate system model of intermediate complexity. Part I: model description and performance for present climate. *Climate Dynamics* 16, 1–17.
- Petoukhov, V., Claussen, M., Berger, A., Crucifix, M., Eby, M., Eliseev, A.V., Fichet, T., Ganopolski, A., Goosse, H., Kamenkovich, I., Mokhov, I.I., Montoya, M., Mysak, L.A., Sokolov, A., Stone, P., Wang, Z., Weaver, A.J., 2005. EMIC Intercomparison Project (EMIP-CO₂): comparative analysis of EMIC simulations of climate, and of equilibrium and transient responses to atmospheric CO₂ doubling. *Climate Dynamics* 25, 363–385. doi:10.1007/s00382-005-0042-3.
- Rahmstorf, S., Crucifix, M., Ganopolski, A., Goosse, H., Kamenkovich, I., Knutti, R., Lohmann, G., Marsh, R., Mysak, L.A., Wang, Z., Weaver, A.J., 2005. Thermohaline circulation hysteresis: a model intercomparison. *Geophysical Research Letters* 32, L23605. doi:10.1029/2005GL023655.
- Ruddiman, W.F., 2003. Orbital insolation, ice volume, and greenhouse gases. *Quaternary Science Reviews* 22, 1597–1629.

- Roche, D.M., Paillard, D., 2005. Modelling the oxygen-18 and rapid glacial climatic events: a data-model comparison. *Comptes Rendus Geoscience* 337, 928–934.
- Roche, D., Paillard, D., Ganopolski, A., Hoffmann, G., 2004a. Oceanic oxygen-18 at the present day and LGM: equilibrium simulations with a coupled climate model of intermediate complexity. *Earth and Planetary Science Letters* 218, 317–330.
- Roche, D., Paillard, D., Cortijo, E., 2004b. Duration and iceberg volume of Heinrich event 4 from isotope modelling study. *Nature* 432, 379–382. doi:10.1038/nature03059.
- Schneider von Deimling, T., Ganopolski, A., Held, H., Rahmstorf, S., 2006. How cold was the Last Glacial Maximum? *Geophysical Research Letters* 33, L14709. doi:10.1029/2006GL026484.
- Shackleton, N.J., 1974. Attainment of isotopic equilibrium between ocean water and the benthonic foraminifera genus *Uvigerina*: isotopic changes in the ocean during the last glacial. *Colloques Internationaux du C.N.R.S* 219, 203–209.
- Siegenthaler, U., Stocker, T.F., Monnin, E., Lüthi, D., Schwander, J., Stauffer, B., Raynaud, D., Barnola, J.-M., Fischer, H., Masson-Delmotte, V., Jouzel, J., 2005. Stable carbon cycle-climate relationship during the Late Pleistocene. *Science* 310, 1313–1317.
- Skinner, L.C., Shackleton, N.J., 2005. An Atlantic lead over Pacific deep-water change across Termination I: implications for the application of the marine isotope stage stratigraphy. *Quaternary Science Reviews* 24, 571–580.
- Stanford, J.D., Rohling, E.J., Hunter, S.E., Roberts, A.P., Rasmussen, S.O., Bard, E., McManus, J., Fairbanks, R.G., 2006. Timing of meltwater pulse 1a and climate responses to meltwater injections. *Paleoceanography* 21, PA4103. doi:10.1029/2006PA001340.
- Stocker, T.F., Johnsen, S.J., 2003. A minimum thermodynamic model for the bipolar seesaw. *Paleoceanography* 18, 1087. doi:10.1029/2003PA000920.
- Stouffer, R.J., Dixon, K.W., Spelman, M.J., Hurlin, W., Yin, J., Gregory, J.M., Weaver, A.J., Eby, M., Flato, G.M., Robitaille, D.Y., Hasumi, H., Oka, A., Hu, A., Jungclaus, J.H., Kamenkovich, I.V., Levermann, A., Montoya, M., Murakami, S., Nawrath, S., Peltier, W.R., Vettoretti, G., Sokolov, A., Weber, S.L., 2006. Investigating the causes of the response of the thermohaline circulation to past and future climate changes. *Journal of Climate* 19, 1365–1387.
- Timmermann, A., Timm, O., Stott, L., Menviel, L., 2009. The roles of CO₂ and orbital forcing in driving southern hemispheric temperature variations during the last 21,000 years. *Journal of Climate* 22, 1626–1640.
- Weaver, A.J., Saenko, O.A., Clark, P.U., Mitrovica, J.X., 2003. Meltwater pulse 1A from Antarctica as a trigger of the Bølling–Allerød warm interval. *Science* 299, 1709–1713.